

HIGHER ORDER UNFITTED SPACE-TIME METHODS FOR TRANSPORT PROBLEMS*

ERIK BURMAN[†] AND FABIAN HEIMANN[‡]

Abstract. In this article, we present an Unfitted Space-Time Finite Element method for the scalar transport equation posed on moving domains. We consider the case of the domain boundary being transported by the same velocity field as the scalar concentration inside the physical domain. A standard continuous Galerkin Finite element space is considered on a fixed background mesh, as well as tensor product Space-Time elements, which can be discontinuous along time slice boundaries. For the computational geometry, we opt for a spatially second-order accurate approximation variant in the mathematical analysis. In particular, we establish stability in a problem-specific norm and prove a priori error bounds of high order. Numerical examples illustrate these theoretical findings.

Key words. moving domains, unfitted FEM, space-time FEM, higher order FEM, transport problems

AMS subject classifications. 65M60, 65M85, 65D30

1. Introduction. Finite Element methods (FEM) provide a powerful framework for the numerical solution of partial differential equations, which appear in a wide range of physical applications, including flow simulations [4, 14]. In this paper, we present a particular novel Finite Element method for the transport (or advection) equation.

In the time-dependent transport problem, an initial concentration function $u_0(x)$ is assumed to be given on a domain $\Omega(t_0) \subset \mathbb{R}^d$, ($d = 1, 2, 3$), which could model for instance a chemical concentration in a droplet. In addition, a transport field \vec{w} is given, and we are interested in solving for a function $u(x, t)$, which describes the concentration after some time t has passed and both species and the overall domain are transported by \vec{w} . We include the case of $\text{div}(\vec{w}) \neq 0$. This physical process can be both seen as a problem of mathematical interest in itself, as well as a relevant model problem for more involved flow simulations, such as Navier-Stokes flows. Note that we also model the limit case of vanishing diffusion of a convection-diffusion problem, which – in comparison – entails some simplifications and challenges.

Drawing from the guiding example of a droplet deforming in a flow process, we focus on the moving domain setup, i.e. we assume the physical domain boundary to be transported with \vec{w} as well. This poses an interesting challenge for formulating a Finite Element method, as these rely on a computational mesh to yield a discrete solution function space. One strategy for handling this complexity, Unfitted Finite Elements (alternative labels include CutFEM, fictitious domain methods) have been developed in the last decades and center around the idea of generating a fixed background mesh on a suitable domain $\tilde{\Omega} \subset \mathbb{R}^d$, where $\Omega(t) \subset \tilde{\Omega}$ for all times t of interest [7]. This allows for a straightforward handling of the computational domain, if stability is ensured by e.g. appropriate stabilisation bilinear forms, and according methods of numerical integration on the cut elements are available.

The approach in this article combines Continuous Galerkin (CG) Finite Elements in space with discontinuous along time slice 1D elements in time. In that way, we derive a space-time Finite Element method of high order, where the meshing task

*Submitted to the editors DATE.

[†]Department of Mathematics, University College London, UK, e.burman@ucl.ac.uk

[‡]Department of Mathematics, University College London, UK, f.heimann@ucl.ac.uk

is solved on a background domain of spatial dimension, and prismatic elements are (implicitly) considered for space and time. Among the innovations of the method is a space-time variant of the Ghost penalty stabilisation, which will solve both stability issues in relation to small cuts and stabilise the weak form of the transport equation as it relates to the use of CG elements in space.

In relation to the discrete geometries, we make use of a specific feature of the physical problem at hand: Because of the straightforward boundary conditions and the locality of the differential operator, we observe that a slight geometrical error in the computational domain as compared to the physical one is not limiting high order convergence of the overall method, assuming initial data and flow field are known on an appropriate neighbourhood of the exact domain. In the Unfitted FE framework, this observation entails that the use of isoparametric mapped elements is not needed, which simplifies the rigorous mathematical analysis. We include the variant method using discrete higher order geometries and isoparametric finite elements in the presentation and numerical examples to set a computational benchmark and illustrate our construction further. (For details on the particulars of the isoparametric mapping considered, we refer the reader to [25, 28, 21].)

As it relates to the mathematical analysis, we establish inf-sup stability of the proposed stabilised bilinear form in a problem specific norm. This implies the unique solvability or well-posedness of the discrete problem. Combining this result with approximation bounds and interpolation errors, we obtain overall a priori error bounds of higher order, which are illustrated by numerical examples. In the L^2 norm, we obtain rigorous estimates of the order $h^{k+\frac{1}{2}}$, whilst numerical experiments show order h^{k+1} for salient families of meshes. Moreover, the theoretical results imply a convergence with h^k in the material derivative norm, which is also observed numerically in the (full space-time) H^1 norm, for simultaneous refinements in space and time respectively.

1.1. Related Methods in the literature. The method at hand relates to the literature on Unfitted Finite Element methods as follows: First, note that relevant techniques in the Unfitted setup had been developed first in the merely spatial case. (C.f. e.g. [7, 10] and the references therein for an overview.) Later, applications of these to time-dependent problems have been studied as well, for a variety of partial differential equations. It is instructive to distinguish time stepping (often also called Eulerian) methods and space-time methods, where the former are based on a spatial discretisation combined with time stepping methods such as Runge-Kutta or BDF schemes, whilst in the latter case finite elements in space and time are employed. As it relates to time stepping methods, the convection-diffusion problem on unfitted moving domains was studied in [27], with higher order generalisations investigated in [29]. The generalisation to Stokes problems was considered in [34, 9]. As for the space-time methods, the convection-diffusion problem was considered in [22, 20, 23, 30, 35, 17, 2]¹. Computational accounts of Navier-Stokes systems moreover were introduced in [1, 16].

Another relevant area of literature relates to the transport equation posed on fixed domains, both for the time-dependent and time-independent variant. Broadly, many methods follow the Discontinuous Galerkin Finite Element approach for these problems. [13, Chapters 2, 3] Lately, also Continuous Galerkin methods including additional stabilisation terms have been developed for related problems. (See e.g. [15, Chapter 61] and the references therein for an overview, or [6] for a recent example

¹Note that most closely related, the present work can be seen as the limit case of diffusion constant $\rightarrow 0$ with respect to [20].

of a Continuous Interior Penalty (CIP) stabilisation variant method.) The particular time-dependent Ghost penalty stabilisation employed in this article can be understood as a member of this broader class of stabilisation variants, now applied to the moving space-time setting.

In relation to the literature background on Ghost penalty stabilisations, we mention the initial work [5]. In the space-time context, a variant of this stabilisation called direct space-time Ghost penalty was developed in [31, 19, 22, 30, 23]. In this article, we adapt the variant of [23, 20] to the case without diffusion and with the dual role of stabilising CG for transport, as well as yielding discrete inequalities on cut meshes relevant for stability.

1.2. Structure of the article. The presentation in the remainder of the article proceeds as follows. In [Section 2](#), we start by putting forward the details of the proposed numerical method. This includes the detailed description of the model problem, which motivates the definition of the bilinear and linear forms. Both uncurved and curved mesh variant methods are introduced. Next, in [Section 3](#) we establish inf-sup stability of the uncurved mesh method. Combining this with interpolation results in [Section 4](#) yields higher order a priori error bounds. In [Section 5](#), numerical examples are provided.

2. Method Introduction. Before introducing the details of the method, we present our problem of consideration.

2.1. Model problem. We are interested in solving the transport or advection equation on moving domains. In particular, let a time interval of interest $t \in [0, T]$ be given, as well as a bounded moving domain $\Omega(t) \subset \mathbb{R}^d, d = 2, 3$, a convection field $\vec{w}(x, t), x \in \Omega(t), t \in [0, T]$, and initial concentration data $u_0(x), x \in \Omega(0)$.² The aim is to model the time evolution of a concentration $u(x, t)$ for $x \in \Omega(t), t \in [0, T]$, where both concentration values at fixed points as well as the domain boundary $\partial\Omega$ are assumed to move with \vec{w} . This function is given as the solution to the following partial differential equation in strong form: Find $u = u(x, t)$ such that

$$(2.1) \quad \begin{aligned} \partial_t u + \operatorname{div}(\vec{w}u) &= f && \text{on } \Omega(t) \quad \forall t \in [0, T], \\ u(x, 0) &= u_0(x) && \text{on } \Omega(0), \end{aligned}$$

where $f = f(x, t)$ represents a right-hand side function modeling sources or sinks. Moreover, we assume that $\Omega(t)$, or $\partial\Omega(t)$, is moving in time with \vec{w} as well. Note that this implies that the formulation [Equation \(2.1\)](#) is well posed insofar as no part of $\partial\Omega(t)$ would need inflow (e.g. Dirichlet) data.³

This particular feature of the problem of interest, needing no boundary data, entails the following observation, which is relevant for motivating our use of a discrete shifted geometry.

LEMMA 2.1 (Extending domain for moving domain transport problem). *Assume a time-dependent domain $\Omega^e(t)$ is given, which has*

$$(2.2) \quad \Omega(t) \subseteq \Omega^e(t) \quad \forall t \in [0, T],$$

together with an extended transport velocity field, \vec{w}^e , defined on $\Omega^e(t)$ with $\vec{w}^e(\cdot, t)|_{\Omega(t)} = \vec{w}(\cdot, t)$, an initial data function u_0^e defined on $\Omega^e(0)$ so that $u_0^e|_{\Omega(0)} = u_0$, and an ex-

²Technicalities about e.g. domains of definition for \vec{w}, u_0 will be given later.

³Compare e.g. to the formulation [13, Eq. (3.1)] and note that for determining the inflow part, the inner product with the relative convection velocity, which vanishes here, needs to be considered.

tended right-hand side f^e defined on $\Omega^e(t)$ with $f^e(\cdot, t)|_{\Omega(t)} = f(\cdot, t)$. Further assume $\partial\Omega^e(t)$ is moving with \bar{w}^e , and let u^e be defined as the solution to the extended problem

$$(2.3) \quad \begin{aligned} \partial_t u^e + \operatorname{div}(\bar{w}^e u^e) &= f^e & \text{on } \Omega^e(t) \quad \forall t \in [0, T], \\ u^e(x, 0) &= u_0^e(x) & \text{on } \Omega^e(0), \end{aligned}$$

Then, denoting by u the solution to [Equation \(2.1\)](#), it holds

$$(2.4) \quad u^e(\cdot, t)|_{\Omega(t)} = u(\cdot, t) \quad \forall t \in [0, T].$$

Proof. The restriction of u^e satisfies [Equation \(2.1\)](#). \square

Let us introduce some notations. First, we assume that the time-dependent domain is given implicitly by a levelset function ϕ :

Assumption 2.2 (Levelset function). There exists a scalar valued function ϕ so that for all $t \in [0, T]$

$$(2.5) \quad \Omega(t) = \{x \in \mathbb{R}^d \mid \phi(x, t) < 0\}.$$

We define the space-time domain as follows

DEFINITION 2.3 (Space-time domain). *The space-time domain $Q \subset \mathbb{R}^{d+1}$ is defined as*

$$(2.6) \quad Q := \bigcup_{t \in [0, T]} \Omega(t) \times \{t\}.$$

Moreover, we define a spatial neighbourhood (or extension by a neighbourhood) of Q for a width parameter $\delta > 0$ as follows:

$$(2.7) \quad U_\delta(Q) := \{(x, t) \in \mathbb{R}^d \times [0, T] \mid \operatorname{dist}_{\mathbb{R}^d}(x, \Omega(t)) < \delta\}.$$

In the light of these notations and motivated by the observation [Lemma 2.1](#), we can make the following assumption on the existence of a strong form solution.

Assumption 2.4. Assume there exists some $\delta > 0$ and a set $U \subset \mathbb{R}^d \times [0, T]$, $U \supseteq U_\delta$, together with functions \bar{w}^e , and f^e defined on U , which extend \bar{w} and f on Q respectively, and a function u_0^e , which extends u_0 on $\Omega(0)$. Moreover, assume that for all $t \in [0, T]$, the spatial boundary $\partial_s U$ moves with \bar{w}^e .⁴

We assume that there exists a solution $u^e \in H^{\operatorname{reg}(u)}(U)$ to the strong form extended problem [Equation \(2.3\)](#), which is bounded as

$$(2.8) \quad \|u^e\|_{H^{\operatorname{reg}(u)}(U)} \lesssim \|u^e\|_{H^{\operatorname{reg}(u)}(Q)}.$$

Here and throughout the article, $\|\cdot\|_{H^k(Q)}$ denotes the usual Sobolev space norm of order k . By $\operatorname{reg}(u)$, we denote an integer parameter for the regularity of u in the space-time Sobolev space manner, to be specified later in the final estimate. Moreover, we use the symbol $A \lesssim B$ to indicate the existence of a constant C independent of exact or discrete geometries so that $A \leq C \cdot B$.⁵ By construction, [Lemma 2.1](#) implies that u^e solves also [Equation \(2.1\)](#).

⁴This part of the assumption is the reason why we allowed for $U \supseteq U_\delta$.

⁵As a further remark on notation, we will only occasionally denote the extended functions f^e , \bar{w}^e , u_0^e with their e index when we want to specifically highlight this aspect. For improved overall readability, whenever any of the three functions is denoted in their non-extended version such as u_0 on a larger domain, it is understood that strictly speaking u_0^e is meant.

2.2. Discrete Method involving uncurved elements. We turn our attention now to formulating the discrete version of this problem. First note that in the Unfitted FE paradigm, the following mesh assumption is salient.

Assumption 2.5 (Unfitted meshes and discrete levelset function). Assume there exists a fixed-in-time polygonal background domain $\tilde{\Omega} \subset \mathbb{R}^d$, so that $\forall t \in [0, T] \Omega(t) \subset \tilde{\Omega}$. Let $T \in \mathcal{T}_h$ be a family of simplicial meshes with maximal element size h on $\tilde{\Omega}$. Denote the interior facets of the mesh as \mathcal{F}_h^i .

In relation to the time discretisation, we assume that the time interval $[0, T]$ is subdivided into elements or time slices I_n of equal width as

$$(2.9) \quad I_n = [t_{n-1}, t_n], \quad \Delta t = t_n - t_{n-1} \quad n = 1, \dots, N, \quad t_0 = 0, t_N = T.$$

We assume that the exact levelset function ϕ is defined on all of $\tilde{\Omega} \times [0, T]$. The discrete geometry is implicitly described in a related manner by an approximate levelset function ϕ^{lin} . We are specifically interested in using the setup of [21] for ϕ^{lin} , which relies on a temporally discrete approximation of ϕ , called ϕ_h . It is of the order q_t in relation to the 1D finite elements in time on I_n . In this article, we assume $q_t \geq 1$. (And give a computational side remark on $q_t = 0$ in Remark 5.1.) Next, ϕ^{lin} is defined for any $t \in [0, T]$ as the elementwise (in relation to the mesh $T \in \mathcal{T}_h$) linear interpolation of ϕ_h . This implies, for instance (see [21] for further details)

$$(2.10) \quad \|\phi - \phi^{\text{lin}}\|_{\infty, \tilde{\Omega} \times [0, T]} \lesssim h^2 + \Delta t^{q_t+1}, \quad \|\nabla \phi - \nabla \phi^{\text{lin}}\|_{\infty, \tilde{\Omega} \times [0, T]} \lesssim h + \Delta t^{q_t+1}.$$

Furthermore, ϕ_h , and by construction then also ϕ^{lin} , shall be continuous in time. Being able to realise this in the general moving domain setup is one of the reasons why we choose at least $q_t = 1$.

The spatially element-wise linear approximation ϕ^{lin} is common in Unfitted Finite Element Methods as it allows for straightforward numerical integration. [7, 24] Specifically, elementwise straight cuts allow for a decomposition of the computational integration domain into few simplices. On these simplices, it is straightforward to map standard Gaussian integration rules. Relating this to the transport problem without essentially any boundary conditions, the piecewise linear discrete geometry presents a good discrete geometry candidate by deviating at most h^2 far and allowing for the mentioned straightforward numerical integration procedure.

Based on ϕ^{lin} , we introduce the following notation for discrete space- and space-time domains:

$$(2.11) \quad \Omega^{\text{lin}}(t) := \{x \in \tilde{\Omega} \mid \phi^{\text{lin}}(x, t) < 0\}, \quad Q^{\text{lin}, n} := \bigcup_{t \in I_n} \Omega^{\text{lin}}(t) \times \{t\}.$$

We denote the extended domain, which is the collection of all elements containing some part of the discrete domain, on a time slice I_n as

$$(2.12) \quad \mathcal{E}(Q^{\text{lin}, n}) := \bigcup \{T \times I_n \mid (T \times I_n) \cap Q^{\text{lin}, n} \neq \emptyset, T \in \mathcal{T}_h\}.$$

Note that because of the asymptotic closeness of ϕ and ϕ^{lin} , for some sufficiently small h and Δt , the domains $Q^{\text{lin}, n}$ and $\mathcal{E}(Q^{\text{lin}, n})$ will be contained in U as in Assumption 2.4. In the following, we assume that h and Δt are always sufficiently small for this set inclusion to hold.

As for the discrete spaces, first assume a spatial polynomial order k_s and a temporal polynomial order k_t are given, which we will sometimes abbreviate as $k = (k_s, k_t)$.

Then, the standard Continuous Galerkin and Discontinuous Galerkin spaces on $\tilde{\Omega}$ are given as

$$(2.13) \quad V_h^{k_s} := \{v \in H^1(\tilde{\Omega}) \mid v|_T \in \mathcal{P}^{k_s}(T) \ \forall T \in \tilde{\mathcal{T}}_h\},$$

$$(2.14) \quad V_{\text{DG}}^{k_s} := \{v \in L^2(\tilde{\Omega}) \mid v|_T \in \mathcal{P}^{k_s}(T) \ \forall T \in \tilde{\mathcal{T}}_h\}.$$

Next, we define the corresponding tensor-product space-time spaces regarding the time interval I_n as

$$(2.15) \quad W_h^{n,(k_s,k_t)} := V_h^{k_s} \otimes \mathcal{P}^{k_t}([t_{n-1}, t_n]), \quad W_{\text{DG}}^{n,(k_s,k_t)} := V_{\text{DG}}^{k_s} \otimes \mathcal{P}^{k_t}([t_{n-1}, t_n]).$$

From the first space, we want to activate those degrees of freedom, which are related to the domain $\mathcal{E}(Q^{\text{lin},n})$ of the respective time slice in order to save unnecessary degrees of freedom for computational reasons. This motivates to define for \mathcal{Q} a space-time domain such as $\mathcal{E}(Q^{\text{lin},n})$

$$(2.16) \quad W_{\text{cut}}^n(\mathcal{Q}) = \{v \in W_h^{n,k} \mid v \text{ vanishes outside of } \mathcal{Q} \text{ as element of } W_h^{n,k}\}.$$

In terms of functions for all time slices, we define in line with the Discontinuous Galerkin in time paradigm

$$(2.17) \quad W_h = \{v \in L^2(\bigcup_{n=1}^N \mathcal{E}(Q^{\text{lin},n})) \mid \forall n = 1, \dots, N : v|_{\mathcal{E}(Q^{\text{lin},n})} \in W_{\text{cut}}^n(\mathcal{E}(Q^{\text{lin},n}))\}$$

For defining the linear and bilinear forms of our method, we will use discrete geometries, which are indicated by an upper index h . As we have opted to use the piecewise linear discrete geometries for our main analysis, we define

$$(2.18) \quad \Omega^h(t) := \Omega^{\text{lin}}(t), \quad Q^{h,n} := Q^{\text{lin},n}, \quad \mathcal{E}(Q^{h,n}) := \mathcal{E}(Q^{\text{lin},n}).$$

Moreover, the global space-time variants should be defined as

$$(2.19) \quad Q^h = \bigcup_{n=1}^N Q^{h,n}, \quad \mathcal{E}(Q^h) = \bigcup_{n=1}^N \mathcal{E}(Q^{h,n}).$$

In terms of these domains, we now introduce the bilinear form of the problem, which contains the physical summand stemming from testing with v and integrating over the domain, and upwind jump penalties as far as DG across time slice boundaries is concerned.

$$(2.20) \quad B_h(u, v) = \sum_{n=1}^N (\partial_t u + \text{div}(\vec{w}u), v)_{Q^{h,n}} + \sum_{n=1}^{N-1} ([u]^n, v_+^n)_{\Omega^h(t_n)} + (u_+^0, v_+^0)_{\Omega^h(t_0)}.$$

Here and in the following, $[u]^n := \lim_{s \searrow t_n} u(s) - \lim_{s \nearrow t_n} u(s)$. Note that the well-posedness of the jump relies on the fact that the discrete domain is continuous, by virtue of the continuity of ϕ^{lin} .

Accordingly, the right-hand side f is given as

$$(2.21) \quad f_h(v) := \sum_{n=1}^N (f, v)_{Q^{h,n}} + (u_0, v_+^0)_{\Omega^h(t_0)}.$$

The bilinear form B_h is complemented by a Ghost-penalty stabilisation bilinear form. We use a space-time version of the direct Ghost penalty as in [31, 19, 22, 23]. It will operate based on interior facets of the mesh $F \in \mathcal{F}_h^i$. Fix any such $F \in \mathcal{F}_h^i$ and let $T_1 \in \mathcal{T}_h$ and $T_2 \in \mathcal{T}_h$ be those elements such that $F = \overline{T_1} \cap \overline{T_2}$. We denote the union of those elements as the facet patch $\omega_F = T_1 \cup T_2$. On this facet patch, we define a jump operator for elementwise polynomials as

$$(2.22) \quad [u]_{\omega_F}|_{T_i}(x, t) = u(x, t) - \mathcal{E}^p(u|_{T_{3-i}})(x, t), \quad i = 1, 2,$$

where \mathcal{E}^p denotes the polynomial extension.

Based on this notation, we define the stabilisation bilinear form contribution from F as

$$(2.23) \quad j_F^n(u, v) := \int_{t_{n-1}}^{t_n} \int_{\omega_F} \gamma_J h^j [u]_{\omega_F} [v]_{\omega_F} dx dt,$$

where γ_J denotes some scalar valued stabilisation parameter and j the integer scaling of the stabilisation. We choose $j = -1$ for this article. The stabilisation shall operate on all facets inside the extended domain, i.e.

$$(2.24) \quad \mathcal{F}^n = \{F \in \mathcal{F} \text{ s.t. } \exists T_1 \neq T_2, T_1 \times I_n, T_2 \times I_n \subseteq \mathcal{E}(Q^{\text{lin}, n}) \text{ with } F = T_1 \cap T_2\}.$$

Summing over all these facets and all time slices, we obtain the overall stabilisation bilinear form

$$(2.25) \quad j_h^n(u, v) = \sum_{F \in \mathcal{F}^n} j_F^n(u, v), \quad J(u, v) = \sum_{n=1}^N j_h^n(u, v).$$

Remark 2.6 (Comparison to Ghost penalty in Convection-Diffusion discretisations). The proposed variant of the direct Ghost penalty is similar to the variants considered in [31, 19, 23, 20] for convection-diffusion problems. We highlight the two relevant differences. First, in the presence of physical diffusion, the scaling j needs to be chosen as $j = -2$. Second, the set of facets, where the Ghost penalty is applied, \mathcal{F}^n is chosen larger in our case to contain both the physical interior and the boundary. This is due to the dual role of the Ghost penalty to stabilise small cut elements and allow for CG elements in space with the transport equation. Because in the convection-diffusion applications the only role of the Ghost penalty is the first one, choosing facets relating to the cut boundary elements suffices in that case.

We can now pose the discrete problem: Find $u_h \in W_h$ such that for all $v_h \in W_h$

$$(2.26) \quad B_h(u_h, v_h) + J(u_h, v_h) = f_h(v_h).$$

2.3. Discrete Method on higher order geometries. The discrete geometries $\Omega^h(t)$, $Q^{h,n}$ as defined above have second order geometrical accuracy. This order of accuracy can be increased to higher order by an isoparametric mapping, see e.g. [21, 23]. When diffusion is involved with according boundary conditions, or initial data or right hand side cannot be extended accordingly, this will be needed to achieve a method of overall high order convergence order. We discuss the according method for the transport equation here as well for computational comparison.⁶

⁶Comparing the rigorous mathematical results of e.g. [20, 23] to the material at hand, we regard the detailed mathematical analysis of the isoparametric method as beyond the scope of this article and leave it as an open question for future research.

Let an isoparametric mapping in space and time be given, $\Theta_h(\cdot, t): \tilde{\Omega} \rightarrow \tilde{\Omega}$, and denote by Θ_h^{st} the space-time version, $\Theta_h^{\text{st}}(x, t) := (\Theta_h(x, t), t)^T$.

In terms of this, we can define the curved discrete regions as

$$(2.27) \quad \Omega^h(t) := \Theta_h(\Omega^{\text{lin}}(t), t), \quad Q^{h,n} := \Theta_h^{\text{st}}(Q^{\text{lin},n}),$$

which shall be understood to replace Equation (2.18) for this subsection. Then, the discrete space W_h is concatenated with the inverse of the mapping (see e.g. [22, 23]), and bilinear form B_h and linear form f_h are given as in Equation (2.20), Equation (2.21), but on the changed higher order discrete domains. Furthermore, the Ghost penalty would be reformulated on curved patches, involving a changed jump operator (see [23, 19] for details).

With these changes in underlying definitions, the discrete problem for the curved meshes / isoparametric method reads the same as Equation (2.26).

3. Discrete Stability and Continuity analysis. In this section, we provide a stability analysis of the formulation Equation (2.26), showing inf-sup stability in particular. This implies the unique solvability of the discrete problem.

To this purpose, we introduce the following discretisation related norms

$$(3.1) \quad |||u|||^2 := \sum_{n=1}^{N-1} ([u]^n, [u]^n)_{\Omega^h(t_n)} + (u_+^0, u_+^0)_{\Omega^h(0)} + (u_-^N, u_-^N)_{\Omega^h(T)}$$

$$(3.2) \quad |||u|||^2 := h \|\partial_t u + w \nabla u\|_{Q^h}^2 + \|u\|_{Q^h}^2 + |||u|||^2$$

$$(3.3) \quad |||u|||_J^2 := |||u|||^2 + J(u, u), \quad |||u|||_J^2 := J(u, u).$$

In the rigorous mathematical analysis, we are interested in the limit behaviour of the method for small mesh sizes h and time steps Δt . In particular, we are interested in simultaneous refinements. We formally assume

Assumption 3.1 (Refinement in h and Δt). We assume h and Δt to be equivalent up to a constant, i.e.

$$(3.4) \quad h \lesssim \Delta t \quad \text{and} \quad \Delta t \lesssim h.$$

Remark 3.2 (Comparison to problem-specific norm in Convection-Diffusion discretisations). We compare the definition of the problem-specific norm $||| \cdot |||$ in this article with the corresponding convection-diffusion analysis presented in [23, 20, 31]. First, the jump summands $||[\cdot]||$ are identical. Next, we have added a volumetric L^2 summand $\|u\|_{Q^{h,n}}^2$ for the transport equation case. This is to balance contributions from $\text{div}(\vec{w}) \neq 0$, at the cost of a constant scaling with $e^{-\alpha T}$ in the stability result. Moreover, this construction allows us to directly control boundary error terms, where in the case of e.g. [20] a more involved trace inequality, using $K \cdot I(\cdot, \cdot)$ summands was needed. Finally, note that in relation to derivatives, we only aim at obtaining control in the material derivative norm in the transport equation, whilst the convection-diffusion analysis was based on separate full $\partial_t u$ and ∇u summands. In this context, Assumption 3.1 also fits in well, yielding a uniform scaling with Δt (or equivalently: h), where in the convection-diffusion case allowing for more general refinements, each of the summands $\partial_t u$ and ∇u was scaled with Δt or h respectively.

Remark 3.3 (Scaling of material derivate in Equation (3.2)). In Equation (3.2), we have opted for a scaling of the material derivative summand of h . In the light of Ass. 3.1, let us mention that this choice would be equivalent to Δt or combinations

such as $t + \frac{h}{\|\vec{w}\|_\infty}$, $\max\{t, \frac{h}{\|\vec{w}\|_\infty}\}$. Depending on different viewpoints any of these might be regarded most natural.

3.1. Discrete Projection Operators. The stability argument we want to put forward involves, for a given discrete function $u \in W_h$, a rescaled version of the space-time discrete function by a smooth scalar function in time, and derivative operators applied to u .⁷ Both of these constructions will not yield a discrete function by themselves. The purpose of the following operators is to remedy this by supplying an appropriate discrete function, together with bounds on the difference incurred.

We start with the case of rescaling of the function $u \in W_h$ by a scalar smooth function φ in time. To yield an appropriate discrete function, we want to apply an L^2 interpolation on each time slice I_n and summarise well-known properties of this operator as follows.

LEMMA 3.4. *For each I_n , there exists an interpolation operator $\Pi^{k_t, n}: V_h^{k_s} \times L^2(I_n) \rightarrow W_{cut}^n(\mathcal{E}(Q^{lin, n}))$, the L^2 interpolation, so that*

$$(3.5) \quad \|\Pi^{k_t, n} u\|_{\mathcal{E}(Q^{lin, n})} \lesssim \|u\|_{\mathcal{E}(Q^{lin, n})}, \quad \|\partial_t \Pi^{k_t, n} u\|_{\mathcal{E}(Q^{lin, n})} \lesssim \|\partial_t u\|_{\mathcal{E}(Q^{lin, n})}.$$

Furthermore, $\Pi^{k_t, n}$ commutes with the spatial derivative, i.e. $\forall u \in V_h^{k_s} \times L^2(I_n)$,

$$(3.6) \quad \nabla(\Pi^{k_t, n} u) = \Pi^{k_t, n}(\nabla u).$$

For a detailed proof of these results, we refer the reader to [31, Lemma 3.15] / [11, Appendix A.1].

We will apply a superconvergence result, which yields a special deviation bound for our argument class of products between a discrete function and a smooth function $\varphi(x, t) = \varphi(t)$. The relevant property is called discrete commutator property. Exploiting the tensor-product structure of $\mathcal{E}(Q^{lin, n})$, we can apply the results from e.g. [3] for a fixed point in space on the respective time element.

LEMMA 3.5. *Let $\varphi \in C^\infty([0, T])$, $u \in W_{cut}^n(\mathcal{E}(Q^{lin, n}))$, then*

$$(3.7) \quad \|\varphi u - \Pi^{k_t, n}(\varphi u)\|_{\mathcal{E}(Q^{lin, n})} \leq C(\varphi) \cdot \Delta t \cdot \|u\|_{\mathcal{E}(Q^{lin, n})},$$

$$(3.8) \quad \|\partial_t(\varphi u - \Pi^{k_t, n}(\varphi u))\|_{\mathcal{E}(Q^{lin, n})} \leq C(\varphi) \cdot \Delta t \cdot \|\partial_t u\|_{\mathcal{E}(Q^{lin, n})}.$$

A global variant of this operator is defined as each $\Pi^{k_t, n}$ on the respective I_n .

DEFINITION 3.6. *The operator Π^{k_t} is defined for arguments $u \in V_h^{k_s} \times L^2([0, T])$ to yield a discrete function $\Pi^{k_t} u \in W_h$ defined by*

$$(3.9) \quad (\Pi^{k_t} u)|_{\hat{\Omega} \times I_n} := \Pi^{k_t, n}(u|_{\hat{\Omega} \times I_n}) \quad \forall n$$

Next, we introduce a further operator, Π_{Osw} , which maps spatially discontinuous Galerkin discrete functions on $\mathcal{E}(Q^{lin, n})$ to corresponding continuous Galerkin functions. It is called Oswald operator in the literature and relies on the idea of averaging out all contributions from degrees of freedom associated to more than one (neighbouring) elements with equal weights. In the notation introduced above, it will map spatial functions from $V_{DG}^{k_s}$ to $V_h^{k_s}$, or the respective temporal tensor products of these spaces. It holds

⁷Details of this can be found below in the proof of Theorem 3.30.

LEMMA 3.7. *For each I_n , there exists an interpolation operator Π_{Osw}^n , so that for each $u \in V_{DG}^{k_s}(\mathcal{E}(\Omega^{lin,n})) \times L^2(I_n)$ we obtain a $\Pi_{Osw}^n(u) \in V_h^{k_s}(\mathcal{E}(\Omega^{lin,n})) \times L^2(I_n)$ such that*

$$(3.10) \quad \|u - \Pi_{Osw}^n u\|_{\mathcal{E}(Q^{lin,n})}^2 \lesssim \int_{I_n} \sum_{F \in \mathcal{F}_n} h_F \| [u] \|_F^2$$

A proof of this property was given in [8].

Again, we define a temporally global variant

DEFINITION 3.8. *The operator Π_{Osw} is defined for arguments $u \in W_{DG}^{n,k}$, $n = 1, \dots, N$ to yield a discrete function $\Pi_{Osw} u \in W_h^{n,k}$, $n = 1, \dots, N$ defined by*

$$(3.11) \quad (\Pi_{Osw} u)|_{\tilde{\Omega} \times I_n} := \Pi_{Osw}^n(u|_{\tilde{\Omega} \times I_n}) \quad \forall n$$

We can relate the facet jump appearing in the upper bound as follows to the Ghost penalty:⁸

LEMMA 3.9. *It holds for $u \in W_{DG}^{n,k}$, $n = 1, \dots, N$*

$$(3.12) \quad \sum_n \int_{I_n} \sum_{F \in \mathcal{F}_n} h_F \| [u] \|_F^2 \lesssim h^{-j} J(u, u)$$

Proof. Fix a time slice I_n and a facet $F \in \mathcal{F}_n$. Let T_1 and T_2 be given such that $F = \bar{T}_1 \cap \bar{T}_2$, and denote $u_1 := u|_{T_1}$, $u_2 := u|_{T_2}$. Then, we can argue

$$(3.13) \quad h_F \| [u] \|_F^2 = h_F \| u_1 - u_2 \|_F^2 \leq h \| u_1 - u_2 \|_{\partial T_i}^2 \lesssim \| \mathcal{E}^p(u_1 - u_2) \|_{T_i}^2 \quad \forall i = 1, 2,$$

where in the last step we applied a standard trace inequality such as [10, Eq. (3.23)]. We can identify this term with the direct Ghost penalty jump and multiply with h^{-j} to cancel out the scaling. \square

This implies for $j = -1$ in particular

COROLLARY 3.10. *It holds*

$$(3.14) \quad \|u - \Pi_{Osw} u\|_{\mathcal{E}(Q^h)}^2 \lesssim h J(u, u).$$

3.2. Ghost-penalty related estimates. The numerical analysis relies on discrete inequalities, which in the cut case are facilitated by the Ghost penalty stabilisation. [7, 10] As it relates to the time-dependent direct Ghost-penalty, in the works [31, 19, 23] such discrete inequalities were established in relation to the scaling $j = -2$, which was applied in the case with diffusion. We present the according results for the general scaling j in the following, in order to apply them to our analysis involving $j = -1$ afterwards.⁹

LEMMA 3.11. *It holds for every $u \in W_h$,*

$$(3.15) \quad \|u\|_{\mathcal{E}(Q^{h,n})}^2 \lesssim h^{-j} j_h^n(u, u) + \|u\|_{Q^{h,n}}^2.$$

Remark 3.12. As for the proof, we refer the reader to [31, 23] and note that j_h^n contains the scaling h^j in our setting.

⁸Note that at this occasion, the dual character of the Ghost penalty becomes relevant, as the set of facets used in e.g. [20] would not suffice.

⁹We mention in passing that we switched from bounds over interior elements, as in [31, 23], to upper bounds containing the physical domains, matching the application of these estimates later.

LEMMA 3.13. *For any $u \in W_h$, $n = 1, \dots, N$, it holds*

$$(3.16) \quad \begin{aligned} (u_+^{n-1}, u_+^{n-1})_{\Omega^h(t_{n-1}^+)} + (u_-^n, u_-^n)_{\Omega^h(t_n^-)} &\lesssim \frac{1}{\Delta t} \|u\|_{\mathcal{E}(Q^{h,n})}^2 \\ &\lesssim \frac{1}{\Delta t} \left(h^{-j} j_h^n(u, u) + \|u\|_{Q^{h,n}}^2 \right) \end{aligned}$$

LEMMA 3.14. *For any $u \in W_h$, it holds*

$$(3.17) \quad \Delta t^2 (\partial_t u, \partial_t u)_{Q^{h,n}} \lesssim \|u\|_{\mathcal{E}(Q^{h,n})}^2 \lesssim h^{-j} j_h^n(u, u) + \|u\|_{Q^{h,n}}^2,$$

LEMMA 3.15. *For any $u \in W_h$, it holds*

$$(3.18) \quad \Delta t^2 J(\partial_t u, \partial_t u) \lesssim J(u, u)$$

$$(3.19) \quad h^2 J(\nabla u, \nabla u) \lesssim J(u, u)$$

Moreover, we can establish the following new result

LEMMA 3.16. *For any $u \in W_h$, it holds*

$$(3.20) \quad h^2 (\nabla u, \nabla u)_{Q^{h,n}} \lesssim \|u\|_{\mathcal{E}(Q^{h,n})}^2 \lesssim h^{-j} j_h^n(u, u) + \|u\|_{Q^{h,n}}^2,$$

More generally, let $u \in W_h$ be given and $\varphi \in C^\infty([0, T])$, $\varphi > 0$. Then,

$$(3.21) \quad h^2 \|\varphi \nabla u\|_{Q^{h,n}}^2 \lesssim h^{-j} \|\varphi u\|_J^2 + \|\varphi u\|_{Q^{h,n}}^2,$$

Proof. The proof is very similar to the temporal derivative property [Lemma 3.14](#). In a first step, we bound the norm by extending the domain to the tensor-product domain $\mathcal{E}(Q^{h,n})$. There, we can apply for any fixed time the standard discrete inequality in space. Lastly, we employ [Lemma 3.11](#) for moving to the physical domain at the cost of a Ghost penalty summand. Relating to [Equation \(3.21\)](#), we note that all discrete arguments relate to spatial functions, so that the argument generalises for a temporal scaling as stated. \square

3.3. Mass conserving bilinear form and trace inequality. In addition, we define a variant of the bilinear form B_h , called B_{mc} , which stands for mass conserving bilinear form:

$$(3.22) \quad B_{mc}(u, v) = (u, -\partial_t v - \vec{w} \cdot \nabla v)_{Q^h} + \sum_{n=1}^{N-1} -(u_-^n, [v]^n)_{\Omega^h(t_n)} + (u_-^N, v_-^N)_{\Omega^h(t_N)}.$$

This bilinear form could be used in its own right as the computational bilinear form of consideration (c.f. e.g. [\[30, 23\]](#) for the related convection-diffusion case and Paragraph “Mass Conserving variant method” in [Section 5](#) below for a numerical experiment in the transport equation case). For the purposes of this analysis, however, we mostly use it as a theoretical tool to obtain relevant positive norm contributions in the stability from symmetric testing summands.

The difference between those two formulations, which stems from the discrete geometries, can be controlled by the following Lemma.

LEMMA 3.17 (Mass conservation form mismatch). *For all $u, v \in W_h \cup H^1(Q^h)$ the following holds*

$$(3.23) \quad |B(u, v) - B_{mc}(u, v)| \leq C_{3.17} (h + \Delta t) \left(\int_0^T \int_{\partial\Omega^h(t)} uv \, d(\partial\Omega^h(t)) \, dt \right).$$

Proof. We apply the framework of [20] or [23] with $q_s = 1$ (corresponding to $\Theta = \text{Id}$), $q_t \geq 1$. First note that the diffusion summands from B and B_{mc} are identical, so they cancel. Moreover, note that in the convection-diffusion analysis, the case of vanishing divergence was considered. When performing the derivation in the proof of [23], which by and large follows an argument of integration by parts on the space-time domain, one notes that the chosen pairing between B and B_{mc} in this article generalises the result to non-vanishing divergence. \square

For the convenient presentation of such terms, we introduce the following straightforward notation for a norm on the spatial boundary:

$$(3.24) \quad \|u\|_{\partial_s Q^h}^2 := \int_0^T \int_{\partial\Omega^h(t)} u^2 \, d(\partial\Omega^h(t)) \, dt$$

3.4. Physical and discrete material space-time derivatives. In the stability proof, we gain control over a discrete version of the material derivative. Note that for a discrete function $u \in W_h$, $\vec{w} \cdot \nabla u \notin W_h$. To circumvent this, the Oswald operator for projecting spatially DG functions into the CG space is supplemented with a discrete version of \vec{w} as follows:

Assumption 3.18. We assume there exists a spatially elementwise P^1 and temporally on I_n constant function $\vec{w}_1 \in W_h^{n,(1,0)}$, $n = 1, \dots, N$, approximating \vec{w}^e , s.t.

$$(3.25) \quad \|\vec{w}^e - \vec{w}_1\|_{Q_h, \infty} \lesssim h^{\frac{1}{2}}.$$

This is justified by first observing that for h and Δt sufficiently small, on each I_n , w^e will be defined on the tensor product space-time domain $\mathcal{E}(Q^{h,n})$. Then, fixing some $t \in I_n$ we can choose e.g. the spatial FE interpolator such as presented in [4, Eq. (4.4.22)] with $s = 0, m = 1$. Hence, for $d = 2$ we require $\|\nabla \vec{w}^e(\cdot, t)\|_{L^4(Q^h)} < \infty$, and for $d = 3$ $\|\nabla \vec{w}^e(\cdot, t)\|_{L^6(Q^h)} < \infty$. Moreover, fix some $x \in \mathcal{E}(Q^{h,n})$ and assume that $\|\partial_t \vec{w}^e(x, \cdot)\|_\infty < \infty$. Then, picking e.g. the candidate $\vec{w}^e(t_{n-1})$ suffices as by elementary arguments, $\vec{w}^e(t) = \vec{w}^e(t_{n-1}) + \int_{t_{n-1}}^t d\tau \partial_t \vec{w}^e(\cdot, \tau)$, so that $\|\vec{w}^e - \vec{w}^e(t_{n-1})\|_{I_n, \infty} \lesssim \Delta t \|\partial_t \vec{w}^e\|_\infty$.

DEFINITION 3.19. We define the space-time material derivative operator $D_t u$ and a discrete counterpart D_t^h with $D_t^h W_h \subseteq W_h$ as

$$(3.26) \quad D_t u := \partial_t u + \vec{w} \cdot \nabla u, \quad D_t^h u := \partial_t u + \Pi_{Osw}(\vec{w}_1 \cdot \nabla u)$$

Measured in the L^2 norm in space and time over Q^h , we obtain for the difference between the two

LEMMA 3.20. It holds

$$(3.27) \quad h \|D_t u - D_t^h u\|_{Q^h}^2 \lesssim \|u\|_{Q^h}^2 + J(u, u) \lesssim \|u\|_j^2.$$

Proof. We calculate

$$\begin{aligned} h \|\vec{w} \nabla u - \Pi_{Osw}(\vec{w}_1 \nabla u)\|_{Q^h}^2 &\lesssim h \|\vec{w} \nabla u - \vec{w}_1 \nabla u\|_{Q^h}^2 + h \|(\text{Id} - \Pi_{Osw})(\vec{w}_1 \nabla u)\|_{Q^h}^2 \\ &\lesssim h^2 \|\nabla u\|_{Q^h}^2 + h^2 J(\vec{w}_1 \nabla u, \vec{w}_1 \nabla u) \text{ by (3.25), (3.14)} \\ &\lesssim \|u\|_{Q^h}^2 + (h + |\vec{w}_1|_\infty) J(u, u) \text{ by (3.20), (3.19).} \end{aligned}$$

All of these terms are bounded by $\|u\|_j^2$. \square

3.5. Space-Time derivatives of and temporally scaled discrete functions in $||| \cdot |||$. We continue with an estimate on the discrete material derivative in our problem specific norm $||| \cdot |||_j$, as well as a similar bound on the temporally rescaled variant of u . Both of these results will be combined in the stability proof to yield $|||\tilde{v}(u)|||_j \lesssim |||u|||_j$, for $\tilde{v}(u)$ a linear combination of the two.

LEMMA 3.21. *It holds for all $u \in W_h$,*

$$(3.28) \quad |||hD_t^h u|||_j \lesssim |||u|||_j.$$

Proof. We prove the property using squared norms. Starting with the Ghost-penalty summand on the left hand side, we observe

$$\begin{aligned} h^2 \|D_t^h u\|_J^2 &\lesssim h^2 \|\partial_t u\|_J^2 + h^2 \|\Pi_{Osw}(\vec{w}_1 \nabla u)\|_J^2 \\ &\lesssim \underbrace{h^2 J(\partial_t u, \partial_t u)}_{\lesssim J(u, u) \text{ by (3.18)}} + \|\vec{w}_1\|_\infty^2 \underbrace{h^2 J(\nabla u, \nabla u)}_{\lesssim J(u, u) \text{ by (3.19)}} + h^2 \|(\text{Id} - \Pi_{Osw})(\vec{w}_1 \nabla u)\|_J^2. \end{aligned}$$

As $J(u, u)$ is among the summands of $|||u|||_j^2$, it remains to estimate the error of the Oswald interpolator, where we note that the integral over the patches can be bound by the global L^2 norm with h^j scaling:

$$\begin{aligned} h^2 \|(\text{Id} - \Pi_{Osw})(\vec{w}_1 \nabla u)\|_J^2 &\lesssim h^{j+2} \|(\text{Id} - \Pi_{Osw})(\vec{w}_1 \nabla u)\|_{\mathcal{E}(Q^h)}^2 \\ &\lesssim h^2 J(\vec{w}_1 \nabla u, \vec{w}_1 \nabla u) \text{ by (3.14)} \\ &\lesssim \|\vec{w}_1\|_\infty^2 J(u, u) \text{ by (3.19)}. \end{aligned}$$

Taking the two last results together yields

$$(3.29) \quad h^2 \|D_t^h u\|_J^2 \lesssim (1 + \|\vec{w}_1\|_\infty^2) J(u, u) \lesssim J(u, u).$$

Now we can consider the next summand

$$\Delta t^3 \|(\partial_t + w \nabla)(D_t^h u)\|_{Q^h}^2 \lesssim \Delta t^3 \|\partial_t D_t^h u\|_{Q^h}^2 + \Delta t^3 \|\vec{w}\|_\infty^2 \|\nabla(D_t^h u)\|_{Q^h}^2,$$

where in particular

$$\begin{aligned} \Delta t^3 \|\partial_t D_t^h u\|_{Q^h}^2 &\lesssim \Delta t (hJ(D_t^h u, D_t^h u) + \|D_t^h u\|_{Q^h}^2) \text{ by (3.17)} \\ &\lesssim |||u|||_j^2 + \Delta t \|D_t u - D_t^h u\|_{Q^h}^2 \lesssim |||u|||_j^2 \text{ by (3.27), (3.29)}. \end{aligned}$$

and for the other summand,

$$\begin{aligned} \Delta t^3 \|\nabla(D_t^h u)\|_{Q^h}^2 &\lesssim \Delta t (hJ(D_t^h u, D_t^h u) + \|D_t^h u\|_{Q^h}^2) \text{ by (3.20)} \\ &\lesssim |||u|||_j^2 \text{ as before.} \end{aligned}$$

Next, we note that the L^2 volume summand is bounded by triangle inequality and (3.27) as

$$(3.30) \quad h^2 \|D_t^h u\|_{Q^h}^2 \lesssim h \|D_t^h u\|_{Q^h}^2 \lesssim h \|D_t u\|_{Q^h}^2 + h \|D_t u - D_t^h u\|_{Q^h}^2 \lesssim |||u|||_j^2.$$

It remains to estimate $||[hD_t^h u]||^2$. We observe

$$\begin{aligned} (3.31) \quad ||[hD_t^h u]||^2 &\lesssim h^2 \left(\sum_{n=0}^{N-1} \|(D_t^h u)_+^n\|_{\Omega^h(t_n)}^2 + \sum_{n=1}^N \|(D_t^h u)_-^n\|_{\Omega^h(t_n)}^2 \right) \\ &\lesssim h \left(\sum_{n=1}^N h j_h^n (D_t^h u, D_t^h u) + \|D_t^h u\|_{Q^{h,n}}^2 \right) \text{ by (3.16)} \\ &\lesssim h^2 J(D_t^h u, D_t^h u) + h \|D_t^h u\|_{Q^h}^2 \lesssim |||u|||_j^2, \text{ as in (3.29), (3.30). } \square \end{aligned}$$

A similar boundedness property holds for the temporally rescaled discrete version of u , which is a discrete projection of $ue^{-\alpha t}$ for some non-negative scalar α to be defined in detail below.

LEMMA 3.22. *It holds for all $u \in W_h$*

$$(3.32) \quad |||\Pi^{k_t}(ue^{-\alpha t})|||_j \lesssim |||u|||_j.$$

Proof. We prove the property using squared norms. Again, we argue for the summands individually. First, consider

$$(3.33) \quad \begin{aligned} \|\Pi^{k_t}(ue^{-\alpha t})\|_J^2 &\lesssim \|ue^{-\alpha t}\|_J^2 + \|(\text{Id} - \Pi^{k_t})(ue^{-\alpha t})\|_J^2 \\ &\lesssim \|u\|_J^2 + h^j \|(\text{Id} - \Pi^{k_t})(ue^{-\alpha t})\|_{\mathcal{E}(Q^h)}^2 \\ &\lesssim \|u\|_J^2 + C(\alpha) \cdot h \cdot \|u\|_{\mathcal{E}(Q^h)}^2 \text{ by (3.7)} \\ &\lesssim \|u\|_J^2 + \|u\|_{Q^h}^2 \lesssim |||u|||_j^2 \text{ by (3.15).} \end{aligned}$$

In relation to the volume term, by similar arguments,

$$\begin{aligned} \|\Pi^{k_t}(ue^{-\alpha t})\|_{Q^h}^2 &\lesssim \|ue^{-\alpha t}\|_{Q^h}^2 + \|(\text{Id} - \Pi^{k_t})(ue^{-\alpha t})\|_{Q^h}^2 \\ &\lesssim \|u\|_{Q^h}^2 + C(\alpha) \cdot h^2 \cdot \|u\|_{\mathcal{E}(Q^h)}^2 \lesssim |||u|||_j \text{ by (3.7), (3.15).} \end{aligned}$$

Next, we can move from time-slice boundaries to the volume by means of a trace inequality on the boundary of the time interval I_n :

$$(3.34) \quad \begin{aligned} |||[\Pi^{k_t}(ue^{-\alpha t})]||^2 &\lesssim ||[ue^{-\alpha t}]||^2 + ||[(\text{Id} - \Pi^{k_t})(ue^{-\alpha t})]||^2 \\ &\lesssim ||[u]||^2 + \frac{1}{\Delta t} \|(\text{Id} - \Pi^{k_t})(ue^{-\alpha t})\|_{\mathcal{E}(Q^h)}^2 + \Delta t \|\partial_t(\text{Id} - \Pi^{k_t})(ue^{-\alpha t})\|_{\mathcal{E}(Q^h)}^2 \\ &\lesssim ||[u]||^2 + C(\alpha) \cdot h \cdot \|u\|_{\mathcal{E}(Q^h)}^2 + C(\alpha) \cdot h^3 \cdot \|\partial_t u\|_{\mathcal{E}(Q^h)}^2 \text{ by (3.7), (3.8)} \\ &\lesssim |||u|||_j^2 + C(\alpha) \cdot h \cdot (\|u\|_{Q^h}^2 + hJ(u, u)) \lesssim |||u|||_j^2 \text{ by (3.15), (3.17).} \end{aligned}$$

Finally, starting from triangle inequality

$$\begin{aligned} \Delta t \|(\partial_t + w\nabla)\Pi^{k_t}(ue^{-\alpha t})\|_{Q^h}^2 &\lesssim \Delta t \|(\partial_t + w\nabla)(ue^{-\alpha t})\|_{Q^h}^2 \\ &\quad + \Delta t \|(\partial_t + w\nabla)[(\text{Id} - \Pi^{k_t})(ue^{-\alpha t})]\|_{Q^h}^2. \end{aligned}$$

Regarding the first term, we apply product rule yielding

$$\Delta t \|(\partial_t + w\nabla)(ue^{-\alpha t})\|_{Q^h}^2 \lesssim \Delta t \|e^{-\alpha t}(\partial_t + w\nabla)u\|_{Q^h}^2 + \Delta t \alpha^2 \|e^{-\alpha t}u\|_{Q^h}^2 \lesssim |||u|||^2.$$

Regarding the second term, we apply the following respective bounds

$$\begin{aligned} \Delta t \|(\partial_t + w\nabla)[(\text{Id} - \Pi^{k_t})(ue^{-\alpha t})]\|_{Q^h}^2 &\lesssim \Delta t^3 C(\alpha) \|\partial_t u\|_{\mathcal{E}(Q^h)}^2 \text{ by (3.8)} \\ &\quad + \Delta t |w|_\infty^2 \|\nabla[(\text{Id} - \Pi^{k_t})(ue^{-\alpha t})]\|_{Q^h}^2 \\ &\lesssim \Delta t C(\alpha) (\|u\|_{Q^h}^2 + hJ(u, u)) + \Delta t |w|_\infty^2 \|(\text{Id} - \Pi^{k_t})(e^{-\alpha t} \nabla u)\|_{Q^h}^2 \text{ by (3.17), (3.6)} \\ &\lesssim |||u|||_j^2 + \Delta t^3 |w|_\infty^2 C(\alpha) \|\nabla u\|_{\mathcal{E}(Q^h)}^2 \lesssim |||u|||_j^2 \text{ by (3.7), (3.20).} \quad \square \end{aligned}$$

3.6. Symmetric testing. In this subsection, we aim at obtaining control over the symmetric testing contribution in bilinear form and Ghost penalty. We proceed in steps about first testing with $ue^{-\alpha t}$, and then its discrete variant. Before that, we establish a special trace inequality, which is needed to control error terms stemming from the application of [Lemma 3.17](#).

LEMMA 3.23 (Special trace inequality). *For all $u \in W_h \cup H^1(Q^h)$, it holds*

$$(3.35) \quad \|u\|_{\partial_s Q^h}^2 \lesssim h^{-1} \|u\|_{\mathcal{E}(Q^h)}^2 + h \|\nabla u\|_{\mathcal{E}(Q^h)}^2.$$

Specially for $u \in W_h$, we have

$$(3.36) \quad \|u\|_{\partial_s Q^h}^2 \leq \frac{C_{3.36}}{h} (\|u\|_{Q^h}^2 + hJ(u, u)).$$

Proof. We subdivide all parts of the boundary $\partial\Omega^h(t)$ for some $t \in I_n$ onto the respective element $T \in \mathcal{T}_h$ with $T \times I_n \subseteq \mathcal{E}(Q^h)$. There, the following cut trace inequality holds (c.f. for instance [\[10, Eq. \(3.24\)\]](#))

$$(3.37) \quad \|u(\cdot, t)\|_{\partial\Omega^h(t) \cap T}^2 \lesssim h^{-1} \|u(\cdot, t)\|_T^2 + h \|\nabla u(\cdot, t)\|_T^2.$$

Integrating over time yields the estimate. For discrete functions $u \in W_h$, we argue further as follows

$$h^{-1} \|u\|_{\mathcal{E}(Q^h)}^2 + h \|\nabla u\|_{\mathcal{E}(Q^h)}^2 \lesssim h^{-1} \|u\|_{Q^h}^2 + J(u, u) \text{ by } (3.15), (3.20). \quad \square$$

LEMMA 3.24. *There exist a constant $\tilde{C}_{3.36}$, depending on the constant of the special trace inequality and related discrete inequalities, but independent of mesh size h , time step Δt , discrete geometry, or other discretisation parameters, so that it holds that for all $u \in W_h$*

$$(3.38) \quad B_h(u, ue^{-\alpha t}) \geq C_{3.24} e^{-\alpha T} \left(\| [u] \|^2 + (\alpha - |\operatorname{div}(\vec{w})|_\infty - \tilde{C}_{3.36}) \|u\|_{Q^h}^2 \right) - J(u, u).$$

Proof. We start with the insight from [Lemma 3.17](#) and split B_h between B_h and B_{mc} as follows

$$2B_h(u, ue^{-\alpha t}) \geq B_h(u, ue^{-\alpha t}) + B_{mc}(u, ue^{-\alpha t}) - C_{3.17} \cdot h \cdot \|ue^{-\alpha t/2}\|_{\partial_s Q^h}^2.$$

Observing a symmetry between the inner terms,

$$\begin{aligned} & B_h(u, ue^{-\alpha t}) + B_{mc}(u, ue^{-\alpha t}) \\ &= \sum_{n=1}^N (\partial_t u + \operatorname{div}(\vec{w}u), e^{-\alpha t} u)_{Q^{h,n}} - (u, \partial_t(ue^{-\alpha t}) + e^{-\alpha t} \vec{w} \cdot \nabla u)_{Q^{h,n}} \\ & \quad + \sum_{n=1}^{N-1} ([u]^n, (u_+^n - u_-^n) e^{-\alpha t_n})_{\Omega^h(t_n)} + (u_+^0, u_+^0)_{\Omega^h(t_0)} + e^{-\alpha t_N} (u_-^N, u_-^N)_{\Omega^h(t_N)} \\ &= \sum_{n=1}^N (e^{-\alpha t} u, \operatorname{div}(\vec{w}u) - \vec{w} \cdot \nabla u)_{Q^{h,n}} + \alpha (e^{-\alpha t} u, u)_{Q^{h,n}} + \| [ue^{-\alpha t/2}] \|^2 \\ &= \sum_{n=1}^N (e^{-\alpha t} u, (\alpha + \operatorname{div}(\vec{w}))u)_{Q^{h,n}} + \| [ue^{-\alpha t/2}] \|^2. \end{aligned}$$

For the remaining boundary term, we argue as follows

$$\begin{aligned} h \cdot \|ue^{-\alpha t/2}\|_{\partial_s Q^h}^2 &\lesssim \|ue^{-\alpha t/2}\|_{\mathcal{E}(Q^h)}^2 + h^2 \|e^{-\alpha t/2} \nabla u\|_{\mathcal{E}(Q^h)}^2 \text{ by (3.35)} \\ &\lesssim \|ue^{-\alpha t/2}\|_{Q^h}^2 + hJ(u, u) \text{ by (3.21)}. \end{aligned}$$

We can identify the $L^2(Q^h)$ volume term and note that the implicit constant in the J term can be absorbed for h sufficiently small. \square

DEFINITION 3.25. *We choose α as follows*

$$(3.39) \quad \alpha := |\operatorname{div}(\vec{w})|_\infty + \tilde{C}_{3.36} + 2.$$

LEMMA 3.26. *It holds for h sufficiently small that for all $u \in W_h$*

$$(3.40) \quad \begin{aligned} B_h(u, \Pi^{k_t}(ue^{-\alpha t})) &\geq C_{3.26} e^{-\alpha T} \left(\| [u] \|^2 + \|u\|_{Q^h}^2 \right) \\ &\quad - C_{3.26B} \sqrt{h} (h \|D_t^h u\|_{Q^h}^2 + J(u, u)). \end{aligned}$$

Proof. We follow up from the previous result and split the difference apart:

$$B_h(u, \Pi^{k_t}(ue^{-\alpha t})) = B_h(u, ue^{-\alpha t}) + B_h(u, (\Pi^{k_t} - \operatorname{Id})(ue^{-\alpha t})).$$

We investigate in detail

$$\begin{aligned} B_h(u, (\Pi^{k_t} - \operatorname{Id})(ue^{-\alpha t})) &= (\partial_t u + \operatorname{div}(\vec{w}u), (\Pi^{k_t} - \operatorname{Id})(ue^{-\alpha t}))_{Q^h} \\ &\quad + \sum_{n=1}^{N-1} ([u]^n, ((\Pi^{k_t} - \operatorname{Id})(ue^{-\alpha t}))_+^n)_{\Omega^h(t_n)} \\ &\quad + (u_+^0, ((\Pi^{k_t} - \operatorname{Id})(ue^{-\alpha t}))_+^0)_{\Omega^h(t_0)}. \end{aligned}$$

For the volume terms, we argue as follows with Cauchy-Schwarz and Youngs inequality

$$\begin{aligned} |(\partial_t u + \operatorname{div}(\vec{w}u), (\Pi^{k_t} - \operatorname{Id})(ue^{-\alpha t}))_{Q^h}| &\leq \|\partial_t u + \operatorname{div}(\vec{w}u)\|_{Q^h} \|(\Pi^{k_t} - \operatorname{Id})(ue^{-\alpha t})\|_{Q^h} \\ &\leq \frac{h^{3/2}}{2} \|\partial_t u + \operatorname{div}(\vec{w}u)\|_{Q^h}^2 + \frac{h^{-3/2}}{2} \|(\Pi^{k_t} - \operatorname{Id})(ue^{-\alpha t})\|_{Q^h}^2 \\ &\leq \frac{h^{3/2}}{2} \|D_t u\|_{Q^h}^2 + \frac{h^{3/2}}{2} |\operatorname{div}(\vec{w})|_\infty^2 \|u\|_{Q^h}^2 + \frac{h^{-3/2}}{2} \|(\Pi^{k_t} - \operatorname{Id})(ue^{-\alpha t})\|_{\mathcal{E}(Q^h)}^2 \\ &\leq \frac{h^{3/2}}{2} \|D_t u\|_{Q^h}^2 + \left[\frac{h^{3/2}}{2} |\operatorname{div}(\vec{w})|_\infty^2 + \frac{h^{1/2}}{2} C(\alpha) \right] \|u\|_{\mathcal{E}(Q^h)}^2 \text{ by (3.7)} \\ &\leq \frac{h^{3/2}}{2} \|D_t^h u\|_{Q^h}^2 + C\sqrt{h}J(u, u) + \left[\frac{h^{3/2}}{2} |\operatorname{div}(\vec{w})|_\infty^2 + \frac{h^{1/2}}{2} (1 + C(\alpha)) \right] \|u\|_{\mathcal{E}(Q^h)}^2 \text{ by (3.27)} \\ &\leq \frac{h^{3/2}}{2} \|D_t^h u\|_{Q^h}^2 + \frac{C_{3.24}}{4} e^{-\alpha T} \|u\|_{Q^h}^2 + C\sqrt{h}J(u, u) \text{ for } h \text{ sufficiently small.} \end{aligned}$$

The temporal interface terms yield a similar result

$$\begin{aligned} &\left| \sum_{n=1}^{N-1} ([u]^n, ((\Pi^{k_t} - \operatorname{Id})(ue^{-\alpha t}))_+^n)_{\Omega^h(t_n)} + (u_+^0, ((\Pi^{k_t} - \operatorname{Id})(ue^{-\alpha t}))_+^0)_{\Omega^h(t_0)} \right| \\ &\leq \frac{h^{1/2}}{2} \| [u] \|^2 + \frac{h^{-1/2}}{2} \sum_{n=0}^{N-1} \|((\Pi^{k_t} - \operatorname{Id})(ue^{-\alpha t}))_+^n\|_{\Omega^h(t_n)}^2 \\ &\leq \frac{h^{1/2}}{2} \| [u] \|^2 + \frac{h^{1/2}}{2} C(\alpha) \|u\|_{\mathcal{E}(Q^h)}^2 \text{ by (3.34).} \end{aligned}$$

\square

LEMMA 3.27. *For all $u \in W_h$,*

$$(3.41) \quad J(u, \Pi^{k_t}(e^{-\alpha t}u)) \geq \frac{14}{16}e^{-\alpha T}J(u, u) - C\|u\|_{Q^h}^2.$$

Proof. We start with the observation that

$$(3.42) \quad J(u, e^{-\alpha t}u) \geq e^{-\alpha T}J(u, u),$$

as the weighting $e^{-\alpha t}$ will just operate as a temporal scaling inside an integral over time of spatial Ghost penalty norm terms. It is always greater equal $e^{-\alpha T}$, hence the estimate holds.

For the remaining difference, we estimate

$$\begin{aligned} J(u, (Id - \Pi^{k_t})(e^{-\alpha t}u)) &\leq \frac{1}{16}e^{-\alpha T}J(u, u) + 4e^{\alpha T}\|(Id - \Pi^{k_t})(e^{-\alpha t}u)\|_J^2 \\ &\leq \frac{1}{16}e^{-\alpha T}J(u, u) + Ce^{\alpha T}h^j\|(Id - \Pi^{k_t})(e^{-\alpha t}u)\|_{\mathcal{E}(Q^h)}^2 \\ &\leq \frac{1}{16}e^{-\alpha T}J(u, u) + e^{\alpha T}C(\alpha)h\|u\|_{\mathcal{E}(Q^h)}^2 \text{ by (3.7)} \\ &\leq \frac{2}{16}e^{-\alpha T}J(u, u) + e^{\alpha T}C(\alpha)h\|u\|_{Q^h}^2, \end{aligned}$$

for h sufficiently small. \square

COROLLARY 3.28. *It holds $\forall u \in W_h$, and h and Δt sufficiently small*

$$(3.43) \quad \begin{aligned} B_h(u, \Pi^{k_t}(ue^{-\alpha t})) + J(u, \Pi^{k_t}(e^{-\alpha t}u)) &\geq C_{3.28}e^{-\alpha T} \left(\|u\|^2 + \|u\|_{Q^h}^2 + J(u, u) \right) \\ &\quad - C_{3.28B}h^{3/2}\|D_t^h u\|_{Q^h}^2. \end{aligned}$$

3.7. Testing with $D_t u$.

LEMMA 3.29. *It holds for all $u \in W_h$*

$$(3.44) \quad B(u, hD_t^h u) + J(u, hD_t^h u) \geq C_{3.29A}h\|D_t^h u\|_{Q^h}^2 - C_{3.29B} \left(\|u\|^2 + \|u\|_{Q^h}^2 + J(u, u) \right).$$

Proof. The Ghost-penalty summand is first estimated by Cauchy-Schwarz and the insight from Equation (3.29):

$$(3.45) \quad J(u, hD_t^h u) \geq -\sqrt{J(u, u)}\sqrt{J(hD_t^h u, hD_t^h u)} \gtrsim -J(u, u).$$

For the B summand, we observe

$$\begin{aligned} B(u, hD_t^h u) &= h(\partial_t u + \vec{w}\nabla u + \operatorname{div}(\vec{w})u, D_t^h u)_{Q^h} \\ &\quad + h \sum_{n=1}^{N-1} ([u]^n, (D_t^h u)_+^n)_{\Omega^h(t_n)} + h(u_+^0, (D_t^h u)_+^0)_{\Omega^h(t_0)}. \end{aligned}$$

Looking at $h(\partial_t u + \vec{w}\nabla u + \operatorname{div}(\vec{w})u, D_t^h u)_{Q^h}$, we focus on deviations in $D_t u$ and $D_t^h u$:

$$\begin{aligned} h(\partial_t u + \vec{w}\nabla u + \operatorname{div}(\vec{w})u, D_t^h u)_{Q^h} &= h\|D_t^h u\|_{Q^h}^2 + h(D_t u - D_t^h u + \operatorname{div}(\vec{w})u, D_t^h u)_{Q^h} \\ &\gtrsim h\|D_t^h u\|_{Q^h}^2 - h \left(\frac{1}{2\epsilon}\|D_t u - D_t^h u + \operatorname{div}(\vec{w})u\|_{Q^h}^2 + \frac{\epsilon}{2}\|D_t^h u\|_{Q^h}^2 \right) \\ &\gtrsim h\|D_t^h u\|_{Q^h}^2 - h\|D_t u - D_t^h u\|_{Q^h}^2 - h\|\operatorname{div}(\vec{w})u\|_{Q^h}^2 \\ &\gtrsim h\|D_t^h u\|_{Q^h}^2 - (1 + h|\operatorname{div}(\vec{w})|_\infty)\|u\|_{Q^h}^2 - J(u, u) \text{ by (3.27)}. \end{aligned}$$

For the boundary terms, we observe by Cauchy-Schwarz

$$\begin{aligned}
& \left| h \sum_{n=1}^{N-1} ([u]^n, (D_t^h u)_+^n)_{\Omega^h(t_n)} + h(u_+^0, (D_t^h u)_+^0)_{\Omega^h(t_0)} \right| \\
& \leq \| [u] \| \cdot \left(\sum_{n=0}^{N-1} h \| (D_t^h u)_+^n \|_{\Omega^h(t_n)}^2 \right) \\
& \leq \frac{1}{2\epsilon_2} \| [u] \|^2 + \frac{\epsilon_2}{2} \left(\sum_{n=0}^{N-1} h^2 \| (D_t^h u)_+^n \|_{\Omega^h(t_n)}^2 \right) \\
& \lesssim \frac{1}{\epsilon_2} \| [u] \|^2 + \epsilon_2 h^2 J(D_t^h u, D_t^h u) + \epsilon_2 h \| D_t^h u \|_{Q^h}^2 \text{ by (3.31)} \\
& \lesssim \frac{1}{\epsilon_2} \| [u] \|^2 + \epsilon_2 J(u, u) + \epsilon_2 h \| D_t^h u \|_{Q^h}^2 \text{ by (3.29)}.
\end{aligned}$$

We can chose ϵ_2 so that any such negative contributions in $h \| D_t^h u \|_{Q^h}^2$ are sufficiently small as measured against the related positive summand. This establishes the claim. \square

3.8. Stability.

THEOREM 3.30. *The bilinear form $B_h + J$ is inf-sup stable on W_h , i.e. for all $u \in W_h$, there exists a $\tilde{v}(u) \in W_h$ such that*

$$(3.46) \quad B_h(u, \tilde{v}(u)) + J(u, \tilde{v}(u)) \gtrsim e^{-\alpha T} \cdot \|u\|_j \cdot \|\tilde{v}(u)\|_j.$$

Hence, the problem (2.26) is well-posed, i.e. it has a unique discrete solution.

Proof. Let $u \in W_h$ be given. We decide to consider $\tilde{v}(u) = C \cdot \Pi^{k_t}(ue^{-\alpha t}) + e^{-\alpha T} h D_t^h u$, where $C = \frac{C_{3.29A} + C_{3.29B}}{C_{3.28}}$.

First, we can obtain from (3.28) and (3.32) that $\|\tilde{v}(u)\|_j \lesssim \|u\|_j$. Hence, it suffices to show

$$B_h(u, \tilde{v}(u)) + J(u, \tilde{v}(u)) \gtrsim e^{-\alpha T} \cdot \|u\|_j^2.$$

To establish this, we start by linearity

$$\begin{aligned}
& B_h(u, \tilde{v}(u)) + J(u, \tilde{v}(u)) \\
& = C [B_h(u, \Pi^{k_t}(ue^{-\alpha t})) + J(u, \Pi^{k_t}(ue^{-\alpha t}))] + e^{-\alpha T} [B_h(u, h D_t^h u) + J(u, h D_t^h u)] \\
& \geq C C_{3.28} e^{-\alpha T} \left(\| [u] \|^2 + \|u\|_{Q^h}^2 + J(u, u) \right) - C C_{3.28B} h^{3/2} \| D_t^h u \|_{Q^h}^2 \text{ by (3.43), (3.44)} \\
& \quad + e^{-\alpha T} C_{3.29A} h \| D_t^h u \|_{Q^h}^2 - e^{-\alpha T} C_{3.29B} \left(\| [u] \|^2 + \|u\|_{Q^h}^2 + J(u, u) \right).
\end{aligned}$$

With the choice of C mentioned above, we obtain

$$\begin{aligned}
& B_h(u, \tilde{v}(u)) + J(u, \tilde{v}(u)) \\
& \geq (C_{3.29A} + C_{3.29B}) e^{-\alpha T} \left(\| [u] \|^2 + \|u\|_{Q^h}^2 + J(u, u) \right) - C C_{3.28B} h^{3/2} \| D_t^h u \|_{Q^h}^2 \\
& \quad + e^{-\alpha T} C_{3.29A} h \| D_t^h u \|_{Q^h}^2 - e^{-\alpha T} C_{3.29B} \left(\| [u] \|^2 + \|u\|_{Q^h}^2 + J(u, u) \right) \\
& \geq C_{3.29A} e^{-\alpha T} \left(\| [u] \|^2 + \|u\|_{Q^h}^2 + J(u, u) + h \| D_t^h u \|_{Q^h}^2 \right) - C C_{3.28B} h^{3/2} \| D_t^h u \|_{Q^h}^2 \\
& \geq C e^{-\alpha T} \|u\|_j^2, \text{ for } h \text{ suff. small.} \quad \square
\end{aligned}$$

3.9. Continuity. For the purposes of showing continuity, we introduce the following larger norm

$$(3.47) \quad |||u|||_*^2 := |||u|||^2 + \frac{1}{h} \|u\|_{\mathcal{E}(Q^h)}^2 + h \|\nabla u\|_{\mathcal{E}(Q^h)}^2 + \sum_{n=1}^N \|u^n\|_{\Omega^h(t_n)}^2$$

$$(3.48) \quad |||u|||_{*,j}^2 := |||u|||_*^2 + J(u, u).$$

In terms of this norm, we can show

LEMMA 3.31. *For all $u \in W_h + H^1(Q^h)$ and $v \in W_h$, it holds*

$$(3.49) \quad B(u, v) \lesssim |||u|||_* |||v|||.$$

Proof. For the proof, we follow [31, 23] in switching to the mass conserving bilinear form, noting that

$$(3.50) \quad B(u, v) \leq |B_{mc}(u, v)| + |B(u, v) - B_{mc}(u, v)|.$$

For the continuity bound in B_{mc} , we obtain $|B_{mc}(u, v)| \lesssim |||u|||_* |||v|||$ by several applications of Cauchy Schwarz inequality, noting that in particular $|(u, \partial_t v + \vec{w} \cdot \nabla v)_{Q^h}| = |(h^{-1/2}u, h^{1/2}(\partial_t v + \vec{w} \cdot \nabla v))_{Q^h}| \lesssim |||u|||_* \cdot |||v|||$.

For the difference $|B(u, v) - B_{mc}(u, v)|$, we argue as follows

$$(3.51) \quad |B(u, v) - B_{mc}(u, v)| \lesssim h \cdot \|u\|_{\partial_s Q^h} \cdot \|v\|_{\partial_s Q^h} \text{ by (3.23)}$$

$$(3.52) \quad \lesssim h^{1/2} \cdot \|u\|_{\partial_s Q^h} \cdot |||v||| \text{ by (3.36),}$$

where we have used that $v \in W_h$ in the last step. In relation to $u \in H^1(Q^h)$, we argue with Equation (3.35) to obtain

$$(3.53) \quad \|u\|_{\partial_s Q^h} \lesssim h^{-1/2} \|u\|_{\mathcal{E}(Q^h)} + h^{1/2} \|\nabla u\|_{\mathcal{E}(Q^h)} \lesssim |||u|||_*. \quad \square$$

4. A priori error estimate.

4.1. Consistency.

LEMMA 4.1. *Let u^e denote the extended solution to the exact problem (2.3), and $v \in W_h$. Then, it holds*

$$(4.1) \quad B(u^e, v) = f(v).$$

Proof. Note that by virtue of Assumption 2.4, the extended solution u^e satisfies the strong form problem in a pointwise manner also on the discrete domain. Multiplying with a test function and integrating over the domain allows to establish the result, noting that u^e is continuous along time slice boundaries, and satisfies the initial condition. \square

4.2. Interpolation and overall bound.

PROPOSITION 4.2. *Denoting by u^e the solution to the extended continuous problem and by u_h the discrete solution of (2.26), it holds*

$$(4.2) \quad |||u^e - u_h||| \lesssim \inf_{w_h \in W_h} |||u^e - w_h|||_* + \|w_h\|_J.$$

Proof. We combine [Theorem 3.30](#), [Lemma 3.31](#), [Lemma 4.1](#) in the general framework of non-conforming Finite Elements, see e.g. [\[13, Thm 1.35\]](#). (Compare also to [\[31, 23, 20\]](#) for a detailed derivation including $\|w_h\|_J$.) \square

THEOREM 4.3 (A priori error bound). *Denoting by u^e the solution to the extended continuous problem [\(2.3\)](#) of regularity $\text{reg}(u) \geq \min(k_s, k_t) + 2$ and by u_h the discrete solution of [\(2.26\)](#), it holds*

$$(4.3) \quad |||u^e - u_h||| \lesssim h^{\min(k_s, k_t) + \frac{1}{2}} \|u\|_{H^{\min(k_s, k_t) + 2}}.$$

Proof. Starting from [Proposition 4.2](#), we are left with the task of finding interpolation bounds. Specifically, we bound the limit by the discrete function supplied by the interpolation operator introduced in [\[31, 11\]](#). Let us denote the global variant as Π^{k_t, k_s} , or Π^k for $k = (k_t, k_s)$. Then, as shown in [\[11, Thm A5\]](#), it holds in our notation, for sufficiently smooth u ¹⁰

$$(4.4) \quad \|u - \Pi^k u\|_{\mathcal{E}(Q^h)} \lesssim \Delta t^{k_t+1} \|u\|_{H^{k_t+1}(\mathcal{E}(Q^h))} + h^{k_s+1} \|u\|_{H^{k_s+1}(\mathcal{E}(Q^h))},$$

$$(4.5) \quad \|\partial_t(u - \Pi^k u)\|_{\mathcal{E}(Q^h)} \lesssim \Delta t^{k_t} \|u\|_{H^{k_t+1}(\mathcal{E}(Q^h))} + h^{k_s+1} \|u\|_{H^{k_s+2}(\mathcal{E}(Q^h))},$$

$$(4.6) \quad \|\nabla(u - \Pi^k u)\|_{\mathcal{E}(Q^h)} \lesssim \Delta t^{k_t+1} \|u\|_{H^{k_t+1}(\mathcal{E}(Q^h))} + h^{k_s} \|u\|_{H^{k_s+1}(\mathcal{E}(Q^h))}.$$

We use these results to establish the bound in relation to the L^2 in space and time summands of $|||\cdot|||_*$. The material derivative is split by a triangle inequality. Noting the scaling within $|||\cdot|||$ yields exactly order $\min(k_s, k_t) + \frac{1}{2}$.

Next, the norms for jump operators can be bound by the respective fixed time norms. These terms also appear in $|||\cdot|||_*$ individually and are bound by the following estimate from [\[11, Lemma A7\]](#) for any $t \in I_n, n = 1, \dots, N$

$$\|(u - \Pi^k u)(t)\|_{\mathcal{E}(Q^h)_t} \lesssim \Delta t^{k_t + \frac{1}{2}} \|u\|_{H^{k_t+1}(\mathcal{E}(Q^{h,n}))} + \Delta t^{-\frac{1}{2}} h^{k_s+1} \|u\|_{H^{k_s+1}(\mathcal{E}(Q^{h,n}))}.$$

Summing over n and taking into account $h \simeq \Delta t$, the summands are controlled by the same upper bound.

In all cases, the boundedness of the extension u^e is used to transfer control from the extended unfitted domain to the physical one, c.f. [Equation \(2.8\)](#).

Finally, in relation to the Ghost penalty remainder, we can establish

$$(4.7) \quad \|\Pi^k u\|_J \lesssim \sqrt{\gamma_J} h^{k_s+1} \|u\|_{H^{k_s+1}(\mathcal{E}(Q^h))}$$

by the proof technique of [\[31, Prop. 3.26\]](#), noting that our h scaling is one order smaller, $j = -1$, and $h \simeq \Delta t$ in our application. \square

We finally point out that by virtue of the problem specific norm, the following error bound in the material derivative is implied.

COROLLARY 4.4. *Denoting by u^e the solution to the extended continuous problem [\(2.3\)](#) of regularity $\text{reg}(u) \geq \min(k_s, k_t) + 2$ and by u_h the discrete solution of [\(2.26\)](#), it holds*

$$(4.8) \quad \|(\partial_t + \vec{w}\nabla)(u^e - u_h)\|_{Q^h} \lesssim h^{\min(k_s, k_t)} \|u\|_{H^{\min(k_s, k_t) + 2}}.$$

¹⁰Note that as a choice of presentation, we will assume maximal regularity of u when compared with discrete orders.

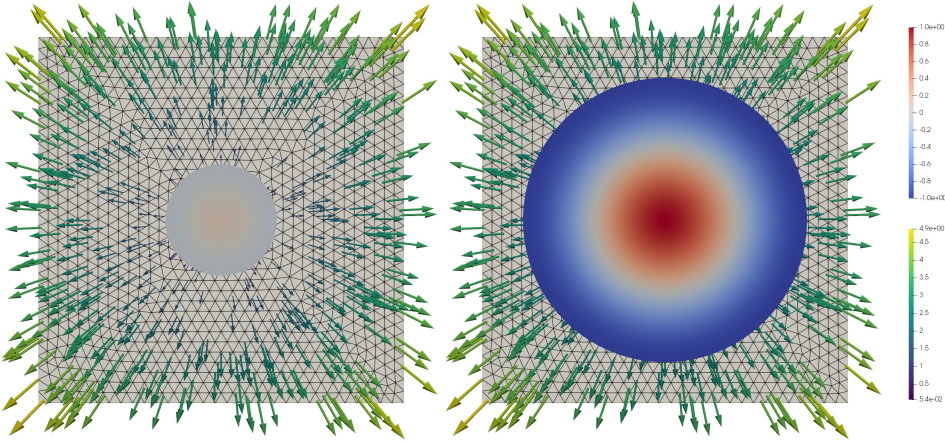


FIG. 1. *Unfitted example geometry in two spatial dimensions. In the background, an unfitted finite element mesh is shown, together with the flow field \vec{w} represented as arrows. In the foreground, the computational geometry with solution function u is displayed. Left: At the end of the first time step, Right: At the end of the final time step.*

5. Numerical Experiments. In this section, we demonstrate the convergence property of the suggested method by numerical experiments. In particular, we prescribe a vector-field \vec{w} , an according moving domain, and a solution function u and calculate the according right hand side f based on the PDE. This allows for straightforward error calculations to assess convergence orders.

All computations are performed with the library `ngsxfem` [26], within the general FE software `NGSolve` [33]. For the resulting linear systems, the direct solvers `Umfpack` [12] and `pardiso` [32] are used.¹¹

5.1. Spatially two dimensional problem. First, let us investigate the method by an example with $\text{div}(w) \neq 0$ in two spatial dimensions. In particular, let $\tilde{\Omega} = [-3.5, 3.5]^2$, $\beta = 1$, and $\vec{w} = \beta(x, y)^T$. The time interval of physical interest shall be $[0, T] = [0, 1]$. In this time, the domain is expanding from a circle centered at the origin with radius 1 to a circle with radius e . This is realised by the following shifted coordinates and time dependent levelset function

$$(5.1) \quad \tilde{x} = \exp(-\beta t)x, \quad \tilde{y} = \exp(-\beta t)y, \quad r = \sqrt{\tilde{x}^2 + \tilde{y}^2}, \quad \phi = r - 1.$$

Note that this geometry satisfies the condition of $\partial\Omega$ moving with \vec{w} . We assume that the solution function u becomes $u = \cos(\pi r) \cdot \sin(\frac{\pi}{2}t)$, and calculate f accordingly in the manufactured solution approach.

The background domain $\tilde{\Omega}$ is equipped with a uniform unstructured mesh of mesh size h . When refining spatial and temporal resolution by means of a parameter $i = 0, 1, \dots$, mesh size and time step are set as $h = 0.9 \cdot (\frac{1}{2})^i$, $\Delta t = T \cdot (\frac{1}{2})^{i+1}$. We illustrate an example mesh, discrete geometry, transport velocity, and time-dependent solution function u in Figure 1. First, we investigate the method with uncurved meshes, which was the focus of the numerical analysis. We fix an order $k = 2, \dots, 6$ and set all discrete space orders to that, $k_s = k_t = k$. For the discrete geometry

¹¹We mention in passing that a computationally similar setup with diffusion was investigated/presented in [22].

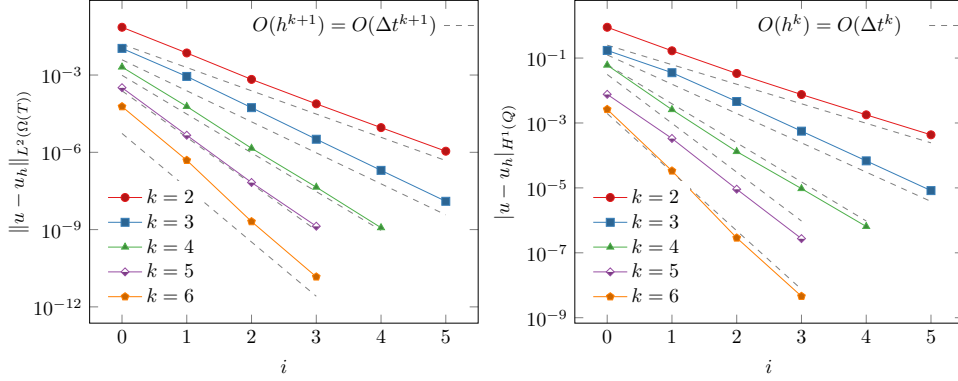


FIG. 2. Convergence of the discrete method for $k = k_s = k_t$ and uncurved meshes in L^2 and H^1 (semi)norms.

order in time, q_t , we chose $q_t = 1$ as the smallest and hence computationally most favourable option. We investigate the convergence of the discrete solution function against the manufactured solution in the following norms:

$$(5.2) \quad \|u - u_h\|_{L^2(\Omega(T))}^2 = \int_{\Omega(T)} (u(T) - u_h(T))^2,$$

$$(5.3) \quad |u - u_h|_{H^1(Q)}^2 = \int_0^T \int_{\Omega(t)} (\nabla u - \nabla u_h)^2 + (\partial_t u - \partial_t u_h)^2$$

The results for these error norms are shown in Figure 2. In terms of the convergence orders, we observe

$$(5.4) \quad \|u - u_h\|_{L^2(\Omega(T))} \simeq h^{k+1} \simeq \Delta t^{k+1}, \quad |u - u_h|_{H^1(Q)} \simeq h^k \simeq \Delta t^k$$

Comparing this to the a priori estimate, we note that the $|\cdot|$ norm is stronger than the combined material derivative contribution in the problem-specific norm, demonstrating the optimality of the theoretical estimate in Corollary 4.4 in relation to the material derivative norm. As it relates to the L^2 scaling, we note that the order observed in numerical experiments is optimal with regards to the interpolation quality. Compared with Theorem 4.3, we observe half an order better numerical performance, but the problem-specific norm was not chosen to yield optimal results in this regard. We leave it as a question for further research whether more exotic meshes could validate the sharpness of the $h^{k+\frac{1}{2}}$ bound.

Remark 5.1 (On $q_t = 0$ and discrete Ghost penalty extensions). When defining the DG in time jump penalties, we have assumed continuity of the discrete geometry in time, to yield straightforward well-posedness of the jump operator. This motivated the choice of $q_t \geq 1$. In the light of the works on CG in [22] or time stepping investigations such as [27], it seems interesting to combine a discontinuous in time discrete geometry stemming from $q_t = 0$ with a Ghost penalty for the purpose of discrete extension of the domain. We mention that from a numerical point of view, the discrete extension mechanism introduced for CG in [22] seems to yield appropriate discrete extensions when combined with the method at hand for $q_t = 0$, but leave a further detailed investigation for future research.

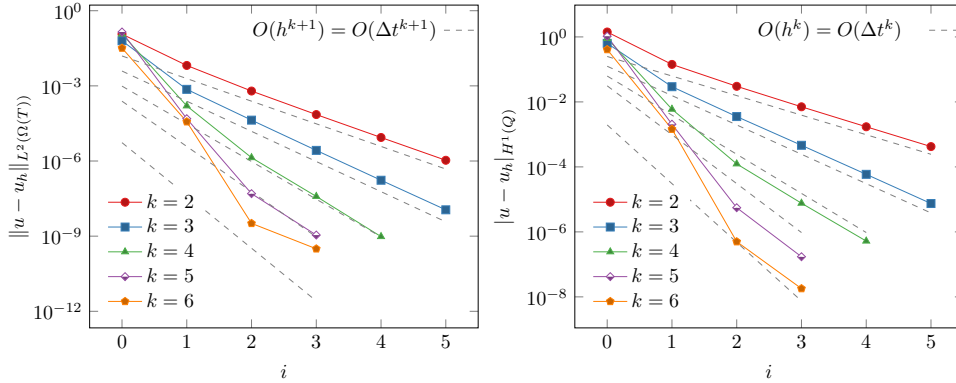


FIG. 3. Convergence of the discrete method for $k = k_s = k_t$ and curved meshes in L^2 and H^1 (semi)norms.

Curved Mesh variant method. Next, we give a numerical comparison to the method with curved meshes, as presented in Subsection 2.3. The discrete errors for the same test case are displayed in Figure 3. We note that the method variant shares the optimal higher order convergence property in the limit h and $\Delta t \rightarrow 0$. However, in the pre-asymptotic regime, the curved meshes seem to negatively affect the absolute numerical errors. This is not uncommon in isoparametric finite elements, but might be seen as a computational argument in favour of the method with uncurved discrete geometries.

Mass Conserving variant method. Paralleling works in the convection-diffusion case [31, 30, 23], one might be interested in considering the straightforward implementation of the method involving the mass conserving bilinear form Equation (3.22). We present the convergence results for the two-dimensional test case for comparison in Figure 4, with uncurved meshes on the left-hand side and isoparametric meshes on the right hand side. Most clearly, the method with uncurved meshes converges only with order \sqrt{h} in the H^1 norm, whilst the curved meshes retain higher order convergence. In the L^2 norm, we observe relatedly (experiments not shown in plots) $h^{3/2}$ with the uncurved meshes and full high order with curved meshes. We conclude that the mass conservative form does not seem suited for a combination with piecewise linear computational geometries, most likely due to a lack of consistency.¹²

5.2. Spatially three dimensional problem. Next, we also demonstrate the applicability of our proposed method to a spatially three dimensional problem, which is motivated by our intended real-life applications in droplets and fluids: In cylindrical coordinates, we chose a parabolic flow profile in a rectangular channel, which will deform a circle geometry into a kite-shaped object, serving as a blueprint for a deformed droplet. We mention in passing that this is a three-dimensional variant/adaptation of the kite geometry of [22, 18].

In particular, let $T = 0.5$, $\Omega = [-1.2, 6] \times [-1.2, 1.2]^2$, $\rho(x, y, z, t) = (10 - y^2 - z^2) \cdot t$, $\vec{w} = (\partial_t \rho, 0, 0)^T$, $r = \sqrt{(x - \rho)^2 + y^2 + z^2}$, $\phi = r - 1$. For this example, we consider the solution $u = \cos(\pi r)$.

¹²We mention in passing that in relation to the blending options of the isoparametric mapping as discussed in detail in [21], we have moved from the Finite Element blending used throughout this study to the smooth blending for the conservative formulation, as we have found it to yield the full orders of convergence for high order applications such as $k = 4$.

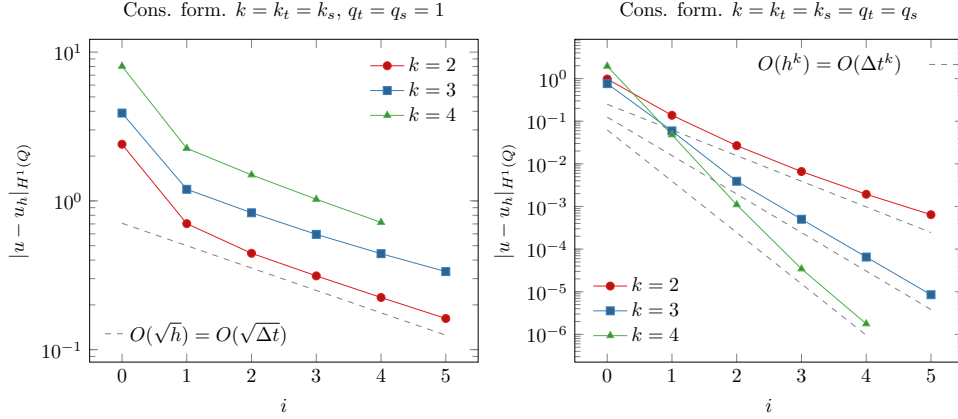


FIG. 4. Convergence of the discrete conservative form method for $k = k_s = k_t$ on uncurved (left hand side) and curved (right hand side) meshes in H^1 seminorm.

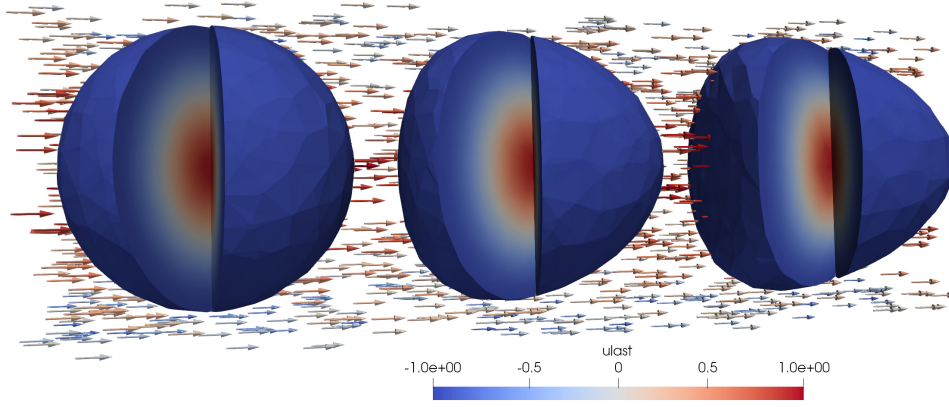


FIG. 5. Flow field \vec{w} (arrows) and discrete solution u for three times instances between $t = 0$ and $t = T$ for the spatially three dimensional problem.

In Figure 5, the computational results for the method involving uncurved meshes is displayed, in particular with $k = 2$. Apart from the validation given by these, we confirm the optimal orders of convergence in a smaller study in Figure 6.

We conclude that our proposed method allows for a straightforward handling of spatially three-dimensional moving objects and leave further applications for future research.

REFERENCES

- [1] M. ANSELMANN AND M. BAUSE, *Cut finite element methods and ghost stabilization techniques for space-time discretizations of the navier–stokes equations*, International Journal for Numerical Methods in Fluids, 94 (2022), pp. 775–802, <https://doi.org/10.1002/fld.5074>, <https://onlinelibrary.wiley.com/doi/abs/10.1002/fld.5074>, <https://arxiv.org/abs/https://onlinelibrary.wiley.com/doi/pdf/10.1002/fld.5074>.
- [2] S. BADIA, H. DILIP, AND F. VERDUGO, *Space-time unfitted finite element methods for*

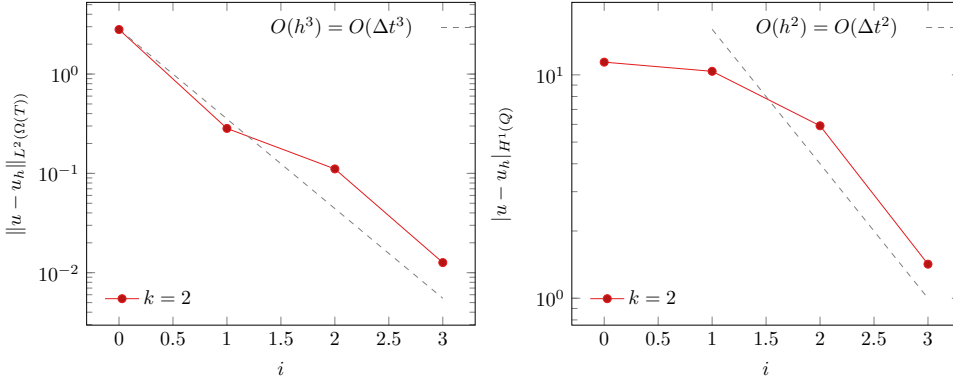


FIG. 6. Convergence of the discrete method for $k = k_s = k_t$ and uncurved meshes in L^2 and H^1 (semi)norms. 3D test case.

- time-dependent problems on moving domains, *Computers & Mathematics with Applications*, 135 (2023), pp. 60–76, <https://doi.org/10.1016/j.camwa.2023.01.032>, <https://www.sciencedirect.com/science/article/pii/S089812212300038X>.
- [3] S. BERTOLUZZA, *The discrete commutator property of approximation spaces*, *Comptes Rendus de l'Académie des Sciences - Series I - Mathematics*, 329 (1999), pp. 1097–1102, [https://doi.org/https://doi.org/10.1016/S0764-4442\(00\)88481-5](https://doi.org/https://doi.org/10.1016/S0764-4442(00)88481-5), <https://www.sciencedirect.com/science/article/pii/S0764444200884815>.
 - [4] S. C. BRENNER AND L. R. SCOTT, *The mathematical theory of finite element methods*, Springer, 2008, <https://doi.org/10.1007/978-0-387-75934-0>.
 - [5] E. BURMAN, *Ghost penalty*, *Comptes Rendus. Mathématique*, 348 (2010), pp. 1217–1220, <https://doi.org/10.1016/j.crma.2010.10.006>.
 - [6] E. BURMAN, *Weighted error estimates for transient transport problems discretized using continuous finite elements with interior penalty stabilization on the gradient jumps*, *Vietnam Journal of Mathematics*, 50 (2022), pp. 833–866, <https://doi.org/10.1007/s10013-022-00550-x>.
 - [7] E. BURMAN, S. CLAUS, P. HANSBO, M. G. LARSON, AND A. MASSING, *Cutfem: discretizing geometry and partial differential equations*, *International Journal for Numerical Methods in Engineering*, 104 (2015), pp. 472–501, <https://doi.org/10.1002/nme.4823>.
 - [8] E. BURMAN AND A. ERN, *Continuous interior penalty hp-finite element methods for advection and advection-diffusion equations*, *Mathematics of Computation*, 76 (2007), pp. 1119–1140.
 - [9] E. BURMAN, S. FREI, AND A. MASSING, *Eulerian time-stepping schemes for the non-stationary Stokes equations on time-dependent domains*, *Numerische Mathematik*, 150 (2022), pp. 423–478, <https://doi.org/10.1007/s00211-021-01264-x>.
 - [10] E. BURMAN, P. HANSBO, M. G. LARSON, AND S. ZAHEDI, *Cut finite element methods*, *Acta Numerica*, 34 (2025), p. 1–121, <https://doi.org/10.1017/S0962492925000017>.
 - [11] E. BURMAN AND J. PREUSS, *Unique continuation for the wave equation based on a discontinuous Galerkin time discretization*, *IMA Journal of Numerical Analysis*, (2025), p. draf036, <https://doi.org/10.1093/imanum/draf036>, <https://doi.org/10.1093/imanum/draf036>, <https://arxiv.org/abs/https://academic.oup.com/imanj/advance-article-pdf/doi/10.1093/imanum/draf036/63408454/draf036.pdf>.
 - [12] T. A. DAVIS, *Algorithm 832: Umfpack v4.3—an unsymmetric-pattern multifrontal method*, *ACM Transactions on Mathematical Software*, 30 (2004), p. 196–199, <https://doi.org/10.1145/992200.992206>.
 - [13] D. A. DI PIETRO AND A. ERN, *Mathematical aspects of discontinuous Galerkin methods*, vol. 69, Springer Science & Business Media, 2011, <https://doi.org/10.1007/978-3-642-22980-0>.
 - [14] A. ERN AND J.-L. GUERMOND, *Finite Elements I*, Springer Cham, 2021, <https://doi.org/10.1007/978-3-030-56341-7>.
 - [15] A. ERN AND J.-L. GUERMOND, *Finite Elements III*, Springer Cham, 2021, <https://doi.org/10.1007/978-3-030-57348-5>.
 - [16] T. FRACHON AND S. ZAHEDI, *A cut finite element method for incompressible two-phase Navier-Stokes flows*, *Journal of Computational Physics*, 384 (2019), pp. 77–98, <https://doi.org/10.1016/j.jcp.2019.01.028>, <https://www.sciencedirect.com/science/>

- article/pii/S0021999119300798.
- [17] P. HANSBO, M. G. LARSON, AND S. ZAHEDI, *A cut finite element method for coupled bulk-surface problems on time-dependent domains*, Computer Methods in Applied Mechanics and Engineering, 307 (2016), pp. 96–116, <https://doi.org/10.1016/j.cma.2016.04.012>.
 - [18] F. HEIMANN, *Implementing cut space-time quadrature rules for three dimensions*. Technical report, University of Göttingen, 04 2019, <https://doi.org/10.25625/STKBWC>.
 - [19] F. HEIMANN, *On Discontinuous- and Continuous-In-Time Unfitted Space-Time Methods for PDEs on Moving Domains*, Master's thesis, University of Göttingen, (2020), <https://doi.org/10.25625/CDCMYT>.
 - [20] F. HEIMANN, *Higher Order Unfitted Space-Time Finite Element Methods for Moving Domain Problems*, PhD thesis, University of Göttingen, 01 2025, <http://dx.doi.org/10.53846/goediss-11003>.
 - [21] F. HEIMANN AND C. LEHRENFELD, *Geometry error analysis of a parametric mapping for higher order unfitted space-time methods*, IMA Journal of Numerical Analysis, (2025, forthcoming), <https://doi.org/10.1093/imanum/drae098>.
 - [22] F. HEIMANN, C. LEHRENFELD, AND J. PREUSS, *Geometrically Higher Order Unfitted Space-Time Methods for PDEs on Moving Domains*, SIAM Journal on Scientific Computing, 45 (2023), pp. pp. B139–B165, <https://doi.org/10.1137/22M1476034>, <https://doi.org/10.1137/22M1476034>.
 - [23] F. HEIMANN, C. LEHRENFELD, AND J. PREUSS, *Discretization error analysis of a high order unfitted space-time method for moving domain problems*, (2025), <https://arxiv.org/abs/2504.08608>, <https://arxiv.org/abs/2504.08608>.
 - [24] C. LEHRENFELD, *On a Space-Time Extended Finite Element Method for the Solution of a Class of Two-Phase Mass Transport Problems*, PhD thesis, RWTH Aachen University, 02 2015, urn:nbn:de:hbz:82-rwth-2015-006739.
 - [25] C. LEHRENFELD, *High order unfitted finite element methods on level set domains using isoparametric mappings*, Computer Methods in Applied Mechanics and Engineering, 300 (2016), pp. 716 – 733, <https://doi.org/10.1016/j.cma.2015.12.005>.
 - [26] C. LEHRENFELD, F. HEIMANN, J. PREUSS, AND H. VON WAHL, ‘ngsxfem’: Add-on to NGSolve for geometrically unfitted finite element discretizations, Journal of Open Source Software, 6 (2021), p. 3237, <https://doi.org/10.21105/joss.03237>.
 - [27] C. LEHRENFELD AND M. A. OLSHANSKII, *An Eulerian finite element method for PDEs in time-dependent domains*, ESAIM: M2AN, 53 (2019), pp. 585–614, <https://doi.org/10.1051/m2an/2018068>.
 - [28] C. LEHRENFELD AND A. REUSKEN, *Analysis of a high order unfitted finite element method for an elliptic interface problem*, IMA Journal of Numerical Analysis, 38 (2018), pp. 1351–1387, <https://doi.org/10.1093/imanum/drx041>.
 - [29] Y. LOU AND C. LEHRENFELD, *Isoparametric unfitted bdf-finite element method for pdes on evolving domains*, SIAM Journal on Numerical Analysis, 60 (2022), pp. 2069–2098, <https://doi.org/10.1137/21M142126X>, <https://doi.org/10.1137/21M142126X>, <https://arxiv.org/abs/https://doi.org/10.1137/21M142126X>.
 - [30] S. MYRBÄCK AND S. ZAHEDI, *A high-order conservative cut finite element method for problems in time-dependent domains*, Computer Methods in Applied Mechanics and Engineering, 431 (2024), p. 117245, <https://doi.org/10.1016/j.cma.2024.117245>, <https://www.sciencedirect.com/science/article/pii/S0045782524005012>.
 - [31] J. PREUSS, *Higher order unfitted isoparametric space-time FEM on moving domains*, Master's thesis, University of Göttingen, (2018), <https://doi.org/10.25625/UACWXS>.
 - [32] O. SCHENK, K. GÄRTNER, W. FICHTNER, AND A. STRICKER, *Pardiso: a high-performance serial and parallel sparse linear solver in semiconductor device simulation*, Future Generation Computer Systems, 18 (2001), pp. 69–78, [https://doi.org/10.1016/S0167-739X\(00\)00076-5](https://doi.org/10.1016/S0167-739X(00)00076-5), <https://www.sciencedirect.com/science/article/pii/S0167739X00000765>. I. High Performance Numerical Methods and Applications. II. Performance Data Mining: Automated Diagnosis, Adaption, and Optimization.
 - [33] J. SCHÖBERL, *C++ 11 Implementation of Finite Elements in NGSolve*, ASC Report, Institute for Analysis and Scientific Computing, Vienna University of Technology, (2014), <https://citeseerx.ist.psu.edu/document?repid=rep1&type=pdf&doi=893a659343ac399679591043b5be8e8ae172772b>.
 - [34] H. VON WAHL, T. RICHTER, AND C. LEHRENFELD, *An unfitted Eulerian finite element method for the time-dependent Stokes problem on moving domains*, IMA Journal of Numerical Analysis, 42 (2021), <https://doi.org/10.1093/imanum/drab044>.
 - [35] S. ZAHEDI, *A space-time cut finite element method with quadrature in time*, in Geometrically Unfitted Finite Element Methods and Applications, S. P. Bordas, E. Burman, M. G. Larson,

and M. A. Olshanskii, eds., Cham, 2017, Springer International Publishing, pp. 281–306,
https://doi.org/10.1007/978-3-319-71431-8_9.